DOI:
10.1021/acsnano.9b04898

Document Version
Peer reviewed version

Neutron Activated ^{153}Sm Sealed in Carbon Nanocapsules for *In Vivo* Imaging and Tumor Radiotherapy

Julie T.-W. Wang[a], Rebecca Klippstein[a], Markus Martincic[b], Elzbieta Pach[c], Robert Feldman[d], Martin Šefl[e,f], Yves Michel[d], Daniel Asker[a], Jane K. Sosabowski[g], Martin Kalbac[h], Tatiana Da Ros[i], Cécilia Ménard-Moyon[j], Alberto Bianco[j], Ioanna Kyriakou[e], Dimitris Emfietzoglou[e], Jean-Claude Saccavini[d], Belén Ballesteros[c,], Khuloud T. Al-Jamal[a,]* and Gerard Tobias[b,]**

[a]Institute of Pharmaceutical Science, King's College London, London SE1 9NH, UK

[b]Institut de Ciència de Materials de Barcelona (ICMAB-CSIC), Campus UAB, 08193 Bellaterra, Barcelona, Spain

[c]Catalan Institute of Nanoscience and Nanotechnology (ICN2), CSIC and the Barcelona Institute of Science and Technology, Campus UAB, 08193 Bellaterra, Barcelona, Spain

[d]Cis Bio International Ion Beam Applications SA, Gif sur Yvette 91192, France

[e]Medical Physics Laboratory, University of Ioannina Medical School, Ioannina GR-45110, Greece

[f]Faculty of Nuclear Sciences and Physical Engineering, Czech Technical University in Prague, Prague 11519, Czech Republic

[g]Centre for Molecular Oncology, Barts Cancer Institute, Queen Mary University of London, London EC1M 6BQ, UK

[h]J. Heyrovsky Institute of the Physical Chemistry, Dolejskova 3, 182 23 Prague 8, Czech Republic

[i]INSTM Unit of Trieste, Department of Chemical and Pharmaceutical Sciences, University of Trieste, Via L. Giorgieri 1, 34127 Trieste, Italy

[j]University of Strasbourg, CNRS, Immunology, Immunopathology and Therapeutic Chemistry, UPR 3572, 67000 Strasbourg, France.

*Corresponding authors E-mail: gerard.tobias@icmab.es, khuloud.al-jamal@kcl.ac.uk, belen.ballesteros@icn2.cat.

ABSTRACT: Radiation therapy along with chemotherapy and surgery remain the main cancer treatments. Radiotherapy can be applied to patients externally (external beam radiotherapy) or internally (brachytherapy and radioisotope therapy). Previously, nanoencapsulation of radioactive crystals within carbon nanotubes, followed by end-closing, resulted in the formation of nanocapsules that allowed ultrasensitive imaging in healthy mice. Herein we report on the preparation of nanocapsules initially sealing 'cold' isotopically enriched samarium (^{152}Sm), which can then be activated on demand to their 'hot' radioactive form (^{153}Sm) by neutron irradiation. The use of 'cold' isotopes avoids the need for radioactive facilities during the preparation of the nanocapsules, reduces radiation exposure to personnel, prevents the generation of nuclear waste and evades the time constraints imposed by the decay of radionuclides. A very high specific radioactivity is achieved by neutron irradiation (up to 11.37 GBq/mg), making the 'hot' nanocapsules useful not only for *in vivo* imaging but also therapeutically effective against lung cancer metastases after intravenous injection. The high *in vivo* stability of the radioactive payload, selective toxicity to cancerous tissues and the elegant preparation method offer a paradigm for application of nanomaterials in radiotherapy.

KEYWORDS: cancer therapy, nuclear imaging, nanoencapsulation, filled carbon nanotubes, radiooncology, nanooncology.

Advances of nanomedicine in cancer diagnosis and therapy require the production of 'small' and 'smart' agents that can offer specific targeting, adequate detection sensitivity, efficient therapeutic effects and ideally favorable biocompatibility.[1-5] Carbon nanotubes (CNTs) have been exploited as delivery systems for theranostic applications.[6-10] Their needle-like structure enables efficient cell penetration.[11-14] Moreover, a selected biomedically relevant payload can be loaded onto the CNT structure either by chemical modification of the largely available external surface (exohedral), or by filling their interior space (endohedral). Surface engineering is a more straightforward approach and has been widely investigated.[15, 16] Although less explored, confinement of imaging and therapeutic agents into CNTs is attracting an increased attention.[17, 18] After encapsulation, the external walls remain available to anchor biocompatible and/or targeting ligands. One advantage of the nanoencapsulation approach is the protection that the carbon coating (CNT walls) offers to the encapsulated materials from enzymatic degradation once exposed to biological environment. It has been already demonstrated that only highly defective, oxidized CNTs are degraded by peroxidases.[19] Apart from CNTs, a variety of materials are being employed for the formation of nanocapsules that shield a selected payload.[20-24] In the vast majority of studies, release of the encapsulated cargo is necessary to achieve a therapeutic effect *via* the delivery of bioactive agents such as drugs. This is however not the case for nuclear imaging and targeted radiotherapy applications where departure of the encaged imaging and/or therapeutic radionuclides from the nanocapsule is neither required nor desired. From the library of nanocapsules available, the properties of carbon nanotubes make them unparalleled for the permanent sealing of radionuclides.[25-28] The graphene shells that constitute the walls of the CNTs can perfectly separate the core from the external environment, forming impermeable nanocapsules when the ends of the CNTs are closed.[29, 30] Having closed ends allows the removal of non-encapsulated material, after

the filling step, under harsh washing conditions[31] and even the retention of gases in their interior.[32] Mutual protection is therefore afforded to both biological systems and the nanotube cargo delivered.[7] When radionuclides are sealed, the action of ionizing particles exerts through the walls of CNTs[25, 27, 28] and it spans from micron to millimeter distances depending on the characteristics of the chosen isotopes. It is worth noting that the internal radionuclides and external moieties (biocompatible/targeting molecules) can be independently changed thus giving versatility to this approach.

In current clinical cancer therapy, half of all cancer patients are treated with radiation therapy either alone or combined with other types of therapies. Nanotechnology strategies however have been mainly driven by the use of chemotherapeutic agents. Notwithstanding, there is a growing interest in the development of nanomaterials bearing radioisotopes, since they offer a platform not only for molecular imaging but also to enhance the radiation response of tumors while reducing side effects.[33-36] CNTs have been shown to deliver positron/γ-radioemitters and alpha particles of interest for imaging and therapeutic applications. This has been mainly achieved *via* chelation of radionuclides onto the external walls[37-39] although the impregnation of radionuclides onto highly defective CNTs, which can be regarded as mesoporous materials, has also been investigated by Wilson *et al*.[40-42] As just mentioned, an attractive feature of CNTs is the possibility to hermetically seal radionuclides in their interior. The nanocapsule will not only prevent release of the chosen radionuclides into the biological milieu but also of their decay products, which might be of a different chemical nature and detach from the nanocarrier with the previously employed strategies. We have previously reported a pioneering work using hermetically sealed Na^{125}I-filled and externally glycosylated single-walled CNTs (SWNT).[25] Specific tissue accumulation (lung) coupled with high *in vivo* stability prevented leakage of radionuclide to high-affinity organs

(thyroid/stomach) or excretion, and resulted in ultrasensitive imaging and delivery of a high radiation dose density[25] Pascu *et al*. have recently given versatility to this approach and investigated the behavior of radiometal-filled (^{64}Cu) SWNT *in vitro* and *in vivo*.[27] In this study the ends of the CNTs were sealed using fullerenes as corks to prevent release of the encapsulated radioemitter.[43, 44] In contrast to these previous reports, where 'hot' radionuclides, in the form of Na^{125}I or ^{64}Cu(OAc)$_2$, were directly filled into SWNT, followed by end-closing, herein, we present an approach by which 'cold' non-radioactive ^{152}Sm is initially sealed into the cavities of both SWNT and multi-walled CNTs (MWNT) leading to the formation of closed-ended ^{152}Sm-filled carbon nanocapsules. The encapsulated and stable ^{152}Sm can then be activated into therapeutically active 'hot' ^{153}Sm by neutron irradiation through the walls of the CNTs (Figure 1a; Schematic representations comparing both strategies to achieve 'hot' nanocapsules are included in Figure S1). After neutron activation, exceptionally high specific activities were obtained, compared to previous works on direct encapsulation of radionuclides, which allowed not only *in vivo* nuclear imaging but also lung tumor radiotherapy. ^{153}Sm is an attractive radionuclide as it emits beta particles at maximum energy of 810 keV (suitable for cell killing), and also releases gamma energy of 103 keV (allowing clinical imaging).[45, 46] ^{153}Sm is used clinically in the form of ^{153}Sm-ethylene diamine tetramethylene phosphonate chelate (^{153}Sm-EDTMP, Quadramet®) for palliation of bone metastases.[47] It offers added advantages such as desirable half-life (46.3 h) and lower gamma energy over other therapeutic radionuclides currently being used in clinic such as iodine-131 or yttrium-90.[48]

The encapsulation of 'hot' radionuclides into the cavity of CNTs requires a fast and safe manipulation of the material due to their constant decay. By using the neutron activation strategy (Figure 1a), both the filling and the removal of the non-encapsulated compound do not require the

use of radioactive facilities thus reducing radiation exposure to the personnel. It also alleviates the time constraints imposed by the constant decay of radionuclides since the 'cold' nanocapsules can be shelf-stored and activated by neutron irradiation on demand. Neutron activation of nanoparticles incorporating neutron-activatable isotopes is well documented, with initial studies focused on the use of fullerenes and polymeric nanoparticles.[49-53] Di Pasqua *et al*. also proposed the use of inorganic mesoporous silica nanoparticles loaded with neutron-activatable holmium-165.[54, 55] Taking advantage of the porosity of the nanocarrier, this was later expanded to chemoradiotherapy.[56] Other inorganic materials including holmium iron garnet, mesoporous carbon nanoparticles and graphene oxide have more recently been explored as holmium nanocarriers.[57-59] On the other hand, neutron activation of large particles (*i.e*. holmium-166 containing microspheres) has been employed in clinical trials for the treatment of liver tumor *via* intra-arterial injection leading to radioembolization.[60, 61] In this work we propose the use of neutron irradiation of 'cold' isotopically enriched ^{152}Sm sealed within carbon nanotubes. The activated 'hot' ^{153}Sm nanocapsules allow both *in vivo* imaging and tumor radiotherapy.

RESULTS AND DISCUSSION

Preparation and neutron activation of ^{152}Sm-filled nanocapsules to yield radioactive ^{153}Sm@CNTs. As-received CNTs were initially purified and shortened by combination of solution processing with strong acids followed by steam.[62] High temperature molten phase capillary filling was employed for the encapsulation of isotopically enriched $^{152}SmCl_3$ into SWNT and MWNT, leading to the closing of the nanotube ends on cooling[29, 30] (Figure 1a). For ease of nomenclature, we will refer to these nanocapsules as ^{152}Sm@SWNT and ^{152}Sm@MWNT. We employed enriched samarium (^{152}Sm) to ensure an efficient activation to the clinically employed ^{153}Sm isotope upon

neutron irradiation.[63] After the filling experiment, the excess of $^{152}SmCl_3$ external to the walls of the CNTs was removed by repeated washings and filtration of the sample in water. The length and external diameter distribution of the samples was determined after the filling step. The median length turned out be *ca*. 200 nm for SWNTs and *ca*. 330 nm for MWNTs (see Figure S2 and Table S1 for statistical data), and the median external diameters 2.1 nm for SWNTs and 10.7 nm for MWNTs (Figure S3, Table S2). The amount of samarium present was next quantitatively determined by ICP-MS. The analyses revealed ~12.3 w/w% and 17.6 w/w% loading of ^{152}Sm for ^{152}Sm@SWNT and ^{152}Sm@MWNT, respectively. The bigger cavity of ^{152}Sm in MWNTs with respect to their single-walled counterparts accounts for the larger amount of encapsulated ^{152}Sm. Due to the large excess of $^{152}SmCl_3$ (10 mg) that was employed for the bulk filling of CNTs (1 mg), only a small fraction of the metal halide was encapsulated (ca. 2 % according to the filling yield). With the present strategy, the non-encapsulated $^{152}SmCl_3$, dissolved during the washing steps, is recovered by filtration. This compound is an enriched non-radioactive form of samarium which can be dried (from the collected filtrate), stored and employed in further filling experiments. Therefore, no samarium waste is generated in the filling step.

Neutron activation is favored in radionuclide production because of its relatively simple process and the availability of various types of nuclear reactors. It also permits lower radiation exposure to the personnel since the preparation procedures such as encapsulation, purification and characterization can be conducted prior to irradiation. Exceptionally high specific radioactivities (SRA) with respect to the mass of the composite material were obtained after 96 h neutron irradiation of ^{152}Sm@SWNTs (6.33 GBq/mg) and ^{152}Sm@MWNT (11.37 GBq/mg) (Table 1). The SRA values are two orders of magnitude (differ by a factor of about 100) higher than those previously reported for neutron irradiated nanocarriers loaded with clinically relevant

radiotherapeutic isotopes, which are in the range of ca. 1-80 MBq/mg (Table S3).[64] This is due to the high neutron flux and long irradiation time employed in the present study taking into account the amount of ^{152}Sm loading. In fact, such high SRA are in line of those achieved by neutron irradiation of pure elements or their oxides for industrial applications.[63]

Structural examination of the nanocapsules before (^{152}Sm@CNT) and after (^{153}Sm@CNT) neutron irradiation. Instant thin-layer chromatography (ITLC) examination was performed for ^{153}Sm@SWNT and ^{153}Sm@MWNT to evaluate whether neutron irradiation had caused any structural damage to the carbon nanocapsules that could result in leakage of ^{152}Sm from their interior. Based on recent studies on non-enriched $SmCl_3$ nanocapsules, over 99% of $SmCl_3$ that is not sealed inside the CNTs can be easily dissolved by a short sonication (10 s) of the sample in water.[65] Therefore, to ensure the complete dissolution of ^{153}Sm from the inner cavities of those CNTs that could have undergone structural damage, a longer sonication step (several min) in water was performed. As shown in Table 1 and Figure S4 a large amount of ^{153}Sm remained sealed in the cavities of MWNT (92%) and SWNT (70%), despite the high neutron flux ($1.6x10^{14}$ n $cm^{-2}s^{-1}$) and long neutron irradiation time employed (96 h) to achieve high SRA. Milder irradiation conditions are usually used to prevent/decrease degradation of the carrier during neutron activation. Comparison of SRA under different conditions is included in Table S1. The fraction of ^{153}Sm external to the CNT walls could be either chelated prior to *in vivo* studies or washed from the sample resulting in a minimal amount of radioactive waste, compared to the previously employed strategy where radionuclides were directly filled into CNTs. The presence of several concentric graphene layers resulted in a more stable construct to the flux of neutrons. Therefore, although ^{152}Sm can be activated inside both MWNT and SWNT, the former turned out to be more robust for the preparation of 'hot' nanocapsules by neutron irradiation. Even higher fractions of

permanently sealed ^{152}Sm would be expected in both constructs by decreasing the time and flux of neutron irradiation, with the corresponding reduction of SRA (according to equation (1)).

Transmission electron microscopy (TEM) allowed us to evaluate the effect of neutron irradiation on the ^{152}Sm-filled CNTs. Encapsulated $^{152}SmCl_3$ can be observed in the high resolution TEM (HRTEM) images of ^{152}Sm@SWNT and ^{152}Sm@MWNT before irradiation (Figure 1b, top panels). The filled metal halides were still present in both types of CNTs (black arrows) after irradiation without evident damage on the nanotube structure. It is important to note that the ends of the carbon nanotubes remain sealed after neutron irradiation (pointed with white arrows). Additional TEM images for both 'cold' and 'hot' nanocapsules are included in Figure S5. Structural changes of the encapsulated crystals are sometimes observed during electron microscopy imaging.[66-71] In the present case we observed that in some cases, $SmCl_3$ nanowires were fragmented into smaller crystals (Figure S6). Preservation of the payload encapsulation was further confirmed by high angle annular dark field (HAADF) scanning transmission electron microscopy (STEM) (Figure 1b, central panels). The $SmCl_3$ filling (bright white lines) aligned nicely within the CNT lumen (dim grey contrast) even following irradiation also indicating the presence of filling material.

Energy dispersive X-ray (EDX) spectroscopy was conducted to assess the preservation of the payload content upon irradiation. The presence of samarium was detected before and after irradiation (Figure 1b, bottom panels). Europium, the decay product of ^{153}Sm, was not detected by EDX because despite the high SRA less than 1% of ^{152}Sm nuclei underwent nuclear reaction to radioactive ^{153}Sm under the employed conditions.

Whole body SPECT/CT imaging and tissue biodistribution of ^{153}Sm@CNTs in normal mice following i.v. injection. The ^{153}Sm@CNT suspensions underwent different dilutions with non-irradiated ^{152}Sm@CNT to contain the appropriate radioactivity for the *in vivo* studies in 1%

Pluronic® F-127 saline. As just discussed, stable nanocapsules sealing 70 % (SWNT) and 92 % (MWNT) of ^{153}Sm were obtained. The sonication step after neutron irradiation ensures no further leakage of ^{153}Sm from the nanocapsules *in vivo*. The fraction of ^{153}Sm dissolved during the preparation of 'hot' nanocapsules was chelated with EDTA to ensure a fast renal clearance.[72] The pharmacokinetics and biodistribution of ^{153}Sm@SWNT and ^{153}Sm@MWNT up to 24 h were next explored by whole body SPECT/CT imaging and quantitative γ-scintigraphy (Figure 2).

SPECT/CT imaging demonstrated that both ^{153}Sm@CNTs showed similar biodistribution patterns with accumulation mostly in spleen, lung and liver within 30 min (Figure 2a). The uptake in these organs was retained up to 24 h post injection (period of imaging). We have previously observed *in vivo* lung accumulation of filled CNTs bearing targeting and non-targeting groups.[25, 28] This behavior has been attributed to the physical properties of CNTs within physiology.[28] As expected, high signals were detected from kidney and bladder within 30 min after injection, which were attributed to the ^{153}Sm:EDTA chelate. From quantitative γ-scintigraphy measurements, a progressive clearance from the blood was observed for both ^{153}Sm@CNTs, in which most of the compounds were cleared out from circulation at 4 h post injection (Figure 2b). Figure 2c shows roughly 20% and 10% of injected dose (ID) were detected in urine in the case of ^{153}Sm@SWNT and ^{153}Sm@MWNT, respectively. The results correlated well with the ITLC findings where a higher amount of free ^{153}Sm was detected after neutron irradiation in ^{153}Sm@SWNT than in ^{153}Sm@MWNT (Figure S4). Negligible radioactivity was detected in feces for both ^{153}Sm@CNTs (< 0.5 %ID). The organ biodistribution profiles established at 4 and 24 h (Figure 2d) paralleled the SPECT/CT imaging results where ^{153}Sm@CNTs largely accumulated in spleen and showed high uptake in lung and liver. The accumulation in spleen and liver increased over time while the uptake

in lung at 4 h and 24 h remained steady. Biodistribution analyses expressed as %ID per organ are presented in Figure S7.

Assessment of radiotherapeutic efficacy of ^{153}Sm@CNTs in B16F10-Luc melanoma lung metastasis. Taking advantage of the prominent lung accumulation property of CNTs, the radiotherapeutic efficacy of ^{153}Sm@SWNT and ^{153}Sm@MWNT was investigated using an experimental B16F10-Luc melanoma lung metastatic tumor model. This syngeneic tumor model is characterized as highly aggressive and metastatic, and has been commonly used for evaluation of cancer regimens.[73, 74] The luciferase-expressing feature of this cell line enabled tumor growth monitoring by whole body bioluminescence imaging.

The results demonstrate that single intravenous administration of 20 MBq of ^{153}Sm@SWNT or ^{153}Sm@MWNT (200 μg of CNTs per mouse) significantly delayed the tumor growth in lung (Figure 3). Representative bioluminescence images of untreated, ^{153}Sm@SWNT and ^{153}Sm@MWNT treated mice on day 10 and day 16 post-tumor inoculation are shown in Figure 3a and images of all mice are shown in Figure S8. From the lung tissues examined at post-mortem (Figure 3b), distinct differences were visualized between the treatment groups. Metastatic melanoma nodules occupied most of the lung tissue from the untreated mice, while lesser number of melanoma nodules were observed in ^{153}Sm@CNT treated mice. The number of tumor nodules also reflected the lung weights in which lung tissues from untreated mice weighed significantly heavier than ^{153}Sm@CNT treated mice (***p<0.001).

Figure 3c displays the average tumor size (photons/sec) of untreated mice and mice treated with ^{153}Sm@SWNT or ^{153}Sm@MWNT over the therapy time course. Treatment responses started to appear on day 13 for both ^{153}Sm@CNTs showing significant tumor reduction compared to the untreated group (*$p < 0.05$). Although similar amount of radioactivity was administered and both

^{153}Sm@CNTs showed comparable % ID in lung, notably smaller tumors were measured in mice treated with ^{153}Sm@SWNT compared to ^{153}Sm@MWNT on day 16 (*$p < 0.05$). Nevertheless, both ^{153}Sm@CNT treatments demonstrated substantial tumor growth suppression on day 16 (***$p <$ 0.001, compared to control) where the therapy study terminated. The reasons behind this more prolonged therapeutic effect of ^{153}Sm@SWNT are not clear, but there might be differences between the two ^{153}Sm@CNTs in terms of the interaction with lung tissues/tumor cells which led to the differential therapeutic outcomes.

Histological analysis was carried out on H&E (hematoxylin and eosin stain) and Neutral Red stained lung tissue sections at post-mortem at the end of therapy study on day 16. The lung sections from untreated mice showed an invasion of cancerous mass leading to the disappearance of healthy lung tissues and a clear reduction of alveoli number (Figure 3d, top panels). In contrast, in ^{153}Sm@CNT treated mice (Figure 3d, middle and bottom panels), lung sections appeared healthier with the presence of fewer colonies of melanoma nodules. Zoom-in images of healthy and cancerous areas from each treatment groups are shown on the right panels with arrows indicating some trapped ^{153}Sm@CNTs. CNTs were difficult to identify in cancerous regions due to the dark appearance of melanoma. Together with the bioluminescence images, it indicated that ^{153}Sm@CNT therapies did not fully eradicate tumors but prevented their proliferation.

Toxicity assessments post ^{153}Sm@CNT injection and after radiotherapy. During the radiotherapy period, variable whole body weight changes were observed within groups (Figure 4a). Body weight loss seemed to occur for the ^{153}Sm@CNT treated mice starting from day 10 post-tumor inoculations but there is no significant difference between the groups including the untreated mice. The weights of major organs were measured at sacrifice. Marginal changes were found between most of the untreated and ^{153}Sm@CNT treated organs, except for lungs (with tumors,

$p < 0.001$) and spleen ($p < 0.01$ or ***$p < 0.001$) (Figure 4b). As previously evidenced in Figure 3b, the aggressively growing tumors increased the weight of lung significantly for the untreated mice. We have previously demonstrated that cold metal-filled CNTs were biocompatible *in vivo*.[75] The significant weight loss in lungs from mice treated with ^{153}Sm@CNTs compared to untreated mice is likely a result of reduction of tumor nodules. Histological assessment performed on mice treated with low dose radioactivity (200 μg ^{153}Sm@CNTs/mouse, 1 MBq) showed no significant histological abnormalities in the selected major organs (heart, lung, kidneys, liver, and spleen) sampled at 24 h post injection (Figure S9). This further confirms that the reduced lung weights were due to the radiotherapy effect and not from the CNTs *per se*.

The average weight of spleen of ^{153}Sm@CNT treated mice was reduced compared to untreated tumor-bearing mice. This is less likely to be general toxicity of the CNTs but a consequence of the high spleen uptake of ^{153}Sm@CNTs leading to high radioactivity accumulation. Histological examination on spleen with profound observation of the death of splenocytes could explain the spleen and body weight reduction of ^{153}Sm@CNT treated mice since the malfunction of spleen can debilitate the immune system (Figure 4c). No histological abnormalities were observed for heart, liver, and kidney. The lack of liver toxicity further supports containments of ^{153}Sm within the CNTs *in vivo*. For example, studies by other groups demonstrated hepatotoxicity with unchelated ^{153}Sm which naturally ends up in reticuloendothelial organs such as the liver and spleen.[47, 72] Hematological and inflammatory examinations are needed in future investigations.

Dosimetry simulation studies. Since the developed therapeutic ^{153}Sm@CNT nanocapsules achieved promising killing effect on tumor cells, a model was established to simulate the performed radiation therapy. Figure 5 shows the comparison between the experimental (green dots) and simulated tumor growth (blue lines, according to equation (2)) data of untreated mice,

and mice treated with ^{153}Sm@SWNT or ^{153}Sm@MWNT. The ^{153}Sm@CNTs were injected on day 8 which is the reason for the hump on the simulated curve at day 8. For both ^{153}Sm@SWNT and ^{153}Sm@MWNT the effect of irradiation was to decrease the rate of tumor growth. Despite the many simplifying assumptions of the model (*e.g.* mono-exponential uptake, washout, and proliferation rates), the simulations reproduced the general trend of the experimental data for both systems. Moreover, the simulations successfully predicted that, for the particular administered activity, biodistribution features and tumor cell type, the resulting dose rate was not high enough. The performed radiotherapy clearly decreased the rate of tumor growth; however, the cell killing could not dominate over cell proliferation which could lead to complete tumor regression. The simulations suggest that local tumor control (defined here as the eradication of all tumor cells with 95% probability) requires roughly 17-28 times higher administered activities (330 MBq for ^{153}Sm@MWNT and 550 MBq for ^{153}Sm@SWNT). Taking into account the obtained SRA values for the prepared nanocapsules, it is indeed possible to administer the required dose for complete eradication of cancer *in vivo* (ca. 30–90 μg of undiluted ^{153}Sm@CNT). In view of efficacy and safety, toxicity profiles using higher doses should be further studied. Due to radiation regulation limits, a much lower dose (20 MBq) has been employed herein for the internal radiation therapy studies. Significant delay in tumor growth has been observed even using such small doses.

CONCLUSIONS

The development of radiopharmaceuticals requires a simple and safe handling of raw materials and final products, during both the manufacturing process, at the point of care, and during the intermediate steps. Furthermore, radiopharmaceuticals must be chosen carefully to deliver the correct activity for the particular radionuclide, given its' half-life. The current work is an original

concept to produce highly energetic ^{153}Sm-encapsulated CNTs *via* a stable intermediate consisting of ^{152}Sm-filled CNT nanocapsules, that may ultimately be used in a therapeutic context. Preparing the CNT nanocapsules in this way enables control over the ^{153}Sm content and consequently, the activity. Furthermore, it reduces the process-complexity and the amount of waste that would be generated if one performed the encapsulation process directly on radioactive isotopes. Finally, the isotopically enriched 'cold' nanocapsules can be stored and activated by neutron irradiation when needed. Neutron irradiation of 'cold' ^{152}Sm-nanocapsules turned out to be robust, especially for MWNT with 92% retention of ^{153}Sm. Extremely high SRA were obtained (6.33 GBq/mg for ^{153}Sm@MWNTs and 11.3 GBq/mg for ^{153}Sm@SWNTs), which allowed live imaging and therapy in experimental metastatic lung tumor model in mice. The obtained SRA are two orders of magnitude higher than those previously reported for neutron activated nanomaterials bearing clinically relevant radioisotopes.[64] On the other hand, the activity of a standard dose of clinically employed yttrium-90 microspheres is 2-4 GBq.[76-78], requiring the administration of over 100 mg (52.0 mCi in 116 mg TheraSphere®).[79] This activity can be achieved with less than 1 mg of the developed nanocapsules. Dosimetry modelling studies can further optimize the treatment efficacy for potential clinical applications and predict the dose required. The preparation of nanocapsules with enriched isotopes benefits from well established filling and end closing strategies, thus giving versatility in the selection of neutron activatable imaging and/or therapeutic isotopes. The possibility of carrying out further surface functionalization on the irradiated nanocapsules can potentially result in a stable nanoconstruct capable of *in vivo* targeting, imaging, and therapy.

METHODS

Additional experimental details are included in the Supporting Information.

Preparation of 'cold' nanocapsules (^{152}Sm@CNT). Both SWNTs and MWNTs (Elicarb®) were initially treated to shorten the tubes, open their ends and remove carbonaceous and metallic (catalyst) impurities. SWNTs were exposed to a combined piranha-steam treatment, whereas MWNTs underwent a combined H_2SO_4:HNO_3-steam treatment following previously reported protocols.[62] Steam is very efficient in removing functional groups and highly defective carbon nanotubes.[62] Enriched $^{152}Sm_2O_3$ (CIS-Bio International-Ion Beam Applications, France) was transformed to anhydrous $^{152}SmCl_3$ following the protocol reported for the synthesis of anhydrous $SmCl_3$ with natural isotopic distribution (non-enriched).[80] The synthesized anhydrous $^{152}SmCl_3$ is highly hygroscopic and was handled under an inert atmosphere, and employed for filling CNTs. SWNT or MWNT and $^{152}SmCl_3$ were ground together in a weight ratio 1:10 (CNTs:$^{152}SmCl_3$) inside an argon filled glove box, split in smaller fractions, placed inside silica tubes and sealed under vacuum. The mixtures were annealed for 12 h at 900 °C (SWNT) or 1200 °C (MWNT) thus leading to the formation of carbon nanocapsules (closed-ended filled CNTs).[29, 30] Removal of the non-encapsulated $^{152}SmCl_3$ with 0.6 M HCl was followed by UV-Vis, until no more $^{152}SmCl_3$ was detected in the washings (0.2 μm Whatman® polycarbonate membranes).[65] The length distribution of the resulting ^{152}Sm@SWNT and ^{152}Sm@MWNT was determined from SEM images, following a previously described methodology,[81] and the external diameter distribution from TEM images. Two hundred CNTs were measured for each of the analyses (see SI).

Neutron activation of ^{152}Sm-filled CNTs to achieve 'hot' nanocapsules (^{153}Sm@CNT). The irradiation protocol was established according to equation (1):[63]

$$A = \frac{0.6\sigma\Phi}{M}\left(1 - e^{-\lambda t}\right) \qquad (1)$$

where A is the predicted activity of the radioisotope produced (Bq g^{-1}), M is the atomic mass of the target element (152 g mol^{-1} for ^{152}Sm), Φ is the neutron flux of the reactor ($1.6x10^{14}$ n $cm^{-2}s^{-1}$), σ is the thermal neutron activation cross-section of the target isotope (206 barns for ^{153}Sm), λ is the decay constant ($0.693/T_{1/2}$), ($T_{1/2}$ is the half life of the target isotope, which is 46.27 h for ^{153}Sm) and *t* is the irradiation time (96 h). Vacuum sealed silica ampoules containing 30 mg of either ^{152}Sm@SWNT or ^{152}Sm@MWNT were placed in an aluminum capsule and irradiated at a neutron flux of $1.6x10^{14}$ n·cm^{-2}·s^{-1} for 96 h in a pool-type reactor (OSIRIS, CEA Saclay, France). ^{153}Sm@SWNT and ^{153}Sm@MWNT powders were separately suspended in a volume of 1% Pluronic® F-127 saline (0.9 % NaCl) solution at 0.5 mg/mL.

Characterization. HAADF-STEM images were acquired at 20 kV on an FEI Magellan XHR Scanning Electron Microscope (SEM). HRTEM images were acquired on a FEI Tecnai G2 F20 microscope at 200 kV. Samples were dispersed in ethanol and deposited onto lacey carbon Cu grids. ^{153}Sm@CNT were imaged after the complete decay of radioactivity. EDX was carried out on a FEI Quanta SEM microscope equipped with an EDAX detector at 20 kV. EDX spectra were acquired on large areas of CNTs (> 50 μm^2) to obtain representative data of the composition of the samples. ICP-MS analysis was carried out using an ICP-MS with a quadrupole collision cell (PerkinElmer Sci EX ELAN® DRC II). Samples for ICP-MS were microwave digested (800 W, 40 min) in a 3:1 mixture of nitric:hydrogen peroxide (Suprapur® Merck KGaA, Germany). For ITLC, aliquots of ^{153}Sm@SWNT and ^{153}Sm@MWNT were spotted on TLC strips (Agilent Technologies, UK) and then developed in 0.1 M ammonium acetate containing 50 mM EDTA as a mobile phase. Strips were allowed to dry and counted quantitatively using a cyclone phosphor detector (Packard Biosciences, UK).

***In vivo* studies.** All *in vivo* experiments were conducted under the authority of project and personal licenses granted by the UK Home Office and the UKCCCR Guidelines (1998). Female C57BL/6 mice aged 6-8 weeks were purchased from Harlan (UK) and used for all *in vivo* studies. Mice were anaesthetized by isoflurane (IsoFlo®, Abbott Laboratorie Ltd, UK) inhalation and injected *via* a tail vein. Each injection dose contained the same amount of CNT (200 μg), and the necessary radioactivity (for imaging, biodistribution or therapy studies) was a by dilution of the ^{153}Sm@CNT suspensions with non-irradiated ^{152}Sm@CNT (2 mg/mL in 1% Pluronic® F-127 saline). Injection suspensions were added with 0.1 M EDTA (one twentieth of the injection volume) to chelate any free ^{153}Sm. For histological examination, collected organs were fixed in 10% neutral buffered formalin. Harvested fixed organs were paraffin-embedded and sectioned for haematoxylin and eosin (H&E) or Neutral Red staining according to standard histological protocols at the Royal Veterinary College (UK). All stained sections were analysed using a Leica DM 1000 LED Microscope (Leica Microsystems, UK) coupled with a CCD digital camera (Qimaging, UK).

***In vivo* imaging, pharmacokinetics and organ biodistribution of ^{153}Sm@CNTs.** Biodistribution was firstly assessed by 3D whole body SPECT/CT imaging (Nano-SPECT/CT, Bioscan, USA). SPECT images were taken in 24 projections over 30-40 min using a four-head scanner with 1.4 mm pinhole collimators. CT scans were performed at the end of each SPECT acquisition. Images were reconstructed by MEDISO software (Medical Imaging Systems), and SPECT and CT images were merged using the InVivoScope™ software (Bioscan, USA). The radioactivity of tissues, blood, urine or feces was measured by γ-scintigraphy (LKB Wallac 1282 Compugamma, PerkinElmer). Blood (sampled from a tail vein), urine and feces were collected over 24 h. To assess the excretion profiles, animals had free access to water but not food.

***In vivo* ^{153}Sm@CNT radiotherapy studies on B16F10-Luc lung metastasis tumor model.** Mice were injected with 5 x 10^5 B16F10-Luc cells in 0.2 mL of PBS *via* a tail vein to establish pulmonary melanoma metastases. Following tumor inoculation, *in vivo* quantitative bioluminescence imaging was performed on day 7, 10, 13 and 16 to monitor the tumor growth (IVIS Lumina III, Perkin-Elmer, UK). Mice were subcutaneously injected with luciferin (D-luciferin potassium salt, Perkin-Elmer, UK) at 150 mg/kg and imaged 10 min after injection. To determine the radiotherapeutic action of ^{153}Sm@CNT, B16F10-Luc tumor bearing C57BL/6 mice were randomly divided into three groups (n = 9-10): untreated, ^{153}Sm@SWNT and ^{153}Sm@MWNT. On day 8 post tumor inoculation, mice were injected with ^{153}Sm@CNT (*ca*. 20 MBq). Mice were sacrificed on day 16 post tumor inoculation, and major organs were collected. Tumor growth was monitored by bioluminescence imaging. The tumor growth data was expressed as mean ± SEM (standard error of the mean), with n denoting the number of animals.

Dosimetry simulation. For targeted radionuclide therapy, the surviving fraction (SF) of the tumor cell population over time, $\mathrm{SF}(t)$, can be described by equation (2).[82]

$$\mathrm{SF}(t) = \exp\left\{-\alpha\, r_0\left(\frac{m-k}{m\,k} + \frac{1}{m}e^{-m\,t} - \frac{1}{k}e^{-k\,t}\right) + \lambda\, t\right\} \qquad (2)$$

where α is the radiosensitivity parameter (Gy^{-1}), r_0 is the extrapolated initial dose rate (Gy h^{-1}), m is the radionuclide effective uptake rate (h^{-1}), k is the radionuclide effective washout rate (h^{-1}) and λ is the tumor cell proliferation rate (h^{-1}). The effective rates of uptake and washout of the radionuclide account for both biological and physical processes and they are defined through $m = \frac{\ln(2)}{T_u} + \frac{\ln(2)}{T_p}$ and $k = \frac{\ln(2)}{T_w} + \frac{\ln(2)}{T_p}$, respectively, where T_u is the biological uptake half-life, T_w is the biological washout half-life, and T_p is the physical half-life of the radionuclide. The values of

m and k were obtained from a fit of the experimental tumor biodistribution data for the percentage injected dose (% ID) using equation (3):

$$\mathrm{ID}(t) = \mathrm{ID}_0 \left(e^{-k\,t} - e^{-m\,t}\right) \qquad (3)$$

where ID_0 is the extrapolated % ID in the tumor at time $t = 0$. Note that the physical half-life of ^{153}Sm ($T_p = 46.3$ h) sets a lower limit to the values of m and k which should be larger than $\frac{\ln(2)}{T_p}$. The least square fits yielded $\mathrm{ID}_0 = 16.6\,\%$, $k = 0.0162\ \mathrm{h}^{-1}$, $m = 2.32\ \mathrm{h}^{-1}$ for SWNTs, and $\mathrm{ID}_0 = 28.0\,\%$, $k = 0.0160\ \mathrm{h}^{-1}$, $m = 0.826\ \mathrm{h}^{-1}$ for MWNTs (Figure S10).

To obtain the rate constant for tumor cell proliferation (λ), we assume (following standard practice) that all tumor cells in the population are proliferating. The experimental tumor growth data of the non-irradiated group of mice are fitted in equation (4):

$$N(t) = N_0\, e^{\lambda\, t}, \qquad (4)$$

where N_0 is the number of tumor cells at $t = 0$. The rate constant λ in equation (4) is normally expressed as $\lambda = \frac{\ln(2)}{T_d}$ with T_d being the tumor doubling time. Fit of the experimental data by equation (4) yields $T_d = 39.78$ h (see Figure 7a).

The extrapolated initial dose rate in the tumor, r_0, entering equation (2) is estimated from equation (5):

$$r_0 = A_0\ \mathrm{ID}_0\ S\ f_T, \qquad (5)$$

where A_0 is the administered activity to the mice (20 MBq), ID_0 is obtained from equation (3), f_T is the fraction of the organ activity that is taken up by the tumor, and S is the radiation absorbed dose to the tumor per radionuclide decay (Gy Bq^{-1} s^{-1}). For ^{153}Sm and a tumor mass of 0.07 g, $S = 4.25\,10^{-10}$ Gy Bq^{-1} s^{-1}.[83] To obtain f_T, it is assumed that the activity was distributed uniformly

in the tumor ($M_{tumor} = 0.07\ g$) and the lungs ($M_{lungs} = 0.12\ g$), so $f_T = \frac{M_{tumor}}{M_{lungs}+M_{tumor}} = 0.368$. Substituting the above parameters in equation (2), the values $r_0 = 3.158\ \text{Gy h}^{-1}$ and $r_0 = 1.872\ \text{Gy h}^{-1}$ are obtained for MWNTs and SWNTs, respectively.

The radiosensitivity parameter α was determined empirically from cell survival data using the expression

$$\alpha = \frac{\ln(\text{SF}_2)}{D + D^2(a/\beta)^{-1}}, \qquad (6)$$

where SF_2 is the measured surviving fraction at $D = 2\ \text{Gy}$ and α/β is the dose where the linear and quadratic cell-kill mechanisms (of the linear-quadratic cell survival model) are equal. For B16F10-Luc cells, $\text{SF}_2 = 0.96$.[84] Such a high value for SF_2 corresponds to an extremely radioresistant cell line. Thus, to a first approximation, we can assume $\alpha/\beta = 1\ \text{Gy}$ which is at the low-end of the range of values observed for the late responding tissues.[85, 86] equation (6) yields $\alpha = 0.0068\ \text{Gy}^{-1}$.

From the above dosimetry model we may also obtain a rough estimate of the required administered activity for local tumor control, defined here as the eradication of all (clonogenic) tumor cells with 95% probability. Assuming that 70 mg of tumor contain roughly 7×10^7 cells (and all are clonogenic) the above local tumor control probability translates to the condition

$$SF < \frac{-\ln(0.95)}{7\times10^7} \approx 7\times10^{-10}$$

which can be achieved with 670 MBq ^{153}Sm@SWNT and 400 MBq ^{153}Sm@MWNT administered activity. If we consider the (perhaps) more realistic approximation that only 1% of tumor cells are clonogenic (*i.e.*,) the $SF < \frac{-\ln(0.95)}{7\times10^5} \approx 7\times10^{-8}$ corresponding administered activity values are 550 MBq ^{153}Sm@SWNT and 330 ^{153}Sm@MWNT.

FIGURES

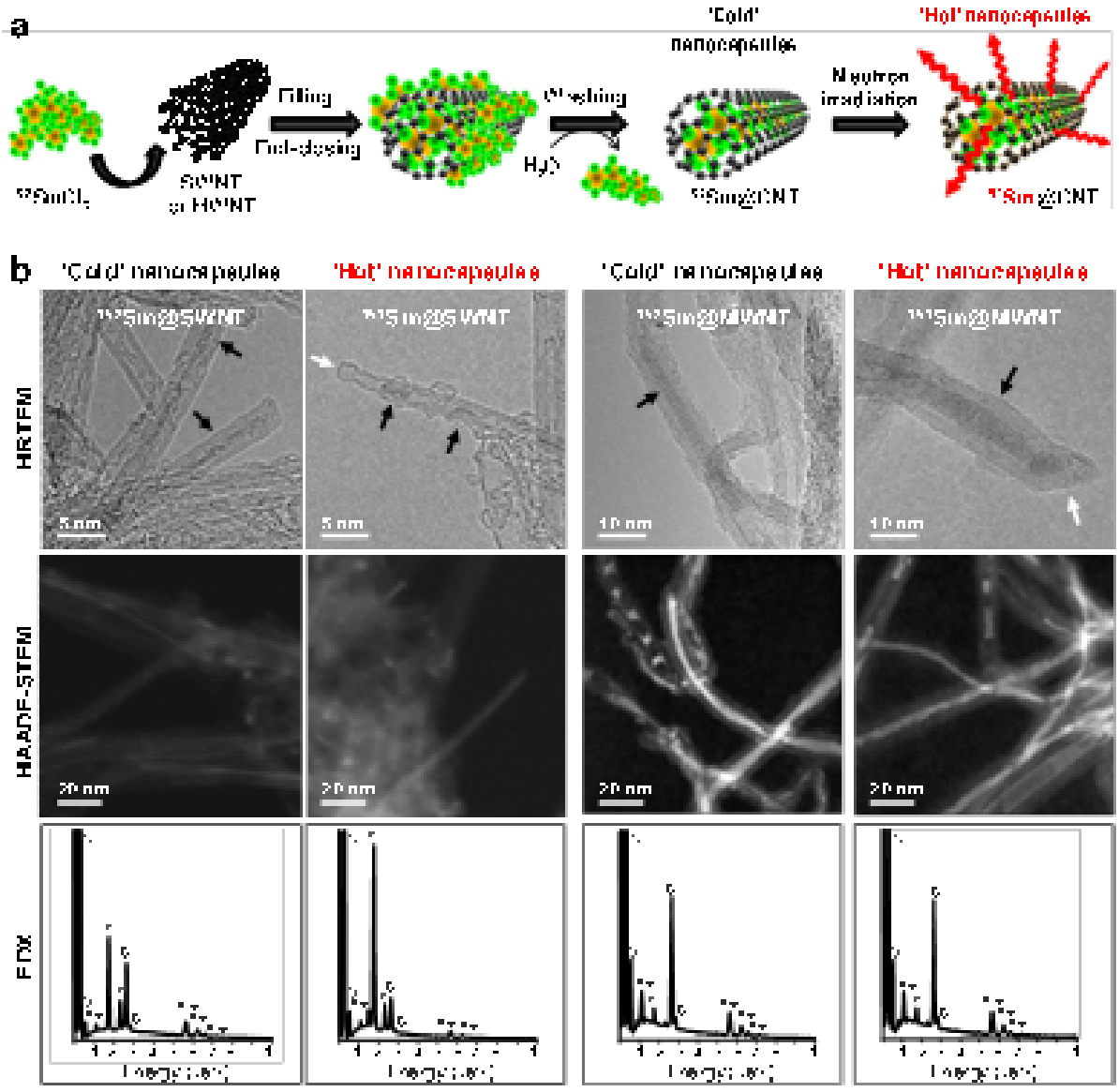

Figure 1. Preparation and characterization of carbon nanocapsules. a) Schematic representation of the strategy employed for the preparation of 'hot' nanocapsules. A non-radioactive enriched precursor is initially encapsulated (^{152}Sm) and it is activated into its radioactive form by neutron irradiation (^{153}Sm) in the last step. The wavy lines indicate radioactivity emerging from radionuclides (^{153}Sm). b) Structural characterization of Sm-filled CNTs before ('Cold' nanocapsules) and after ('Hot' nanocapsules) irradiation. HRTEM images are shown in the top panels. Black arrows point to the $SmCl_3$ filling, and white arrows to closed tips of carbon

nanotubes. The crystalline structure of $SmCl_3$ can be better appreciated on the MWNT images, with visible lattice fringes (parallel lines). HAADF-STEM images are shown in the middle panels. The bright lines correspond to the filling of $SmCl_3$, while CNTs appear as a dim grey contrast. EDX analyses confirming the presence of $SmCl_3$ are shown in the bottom panels.

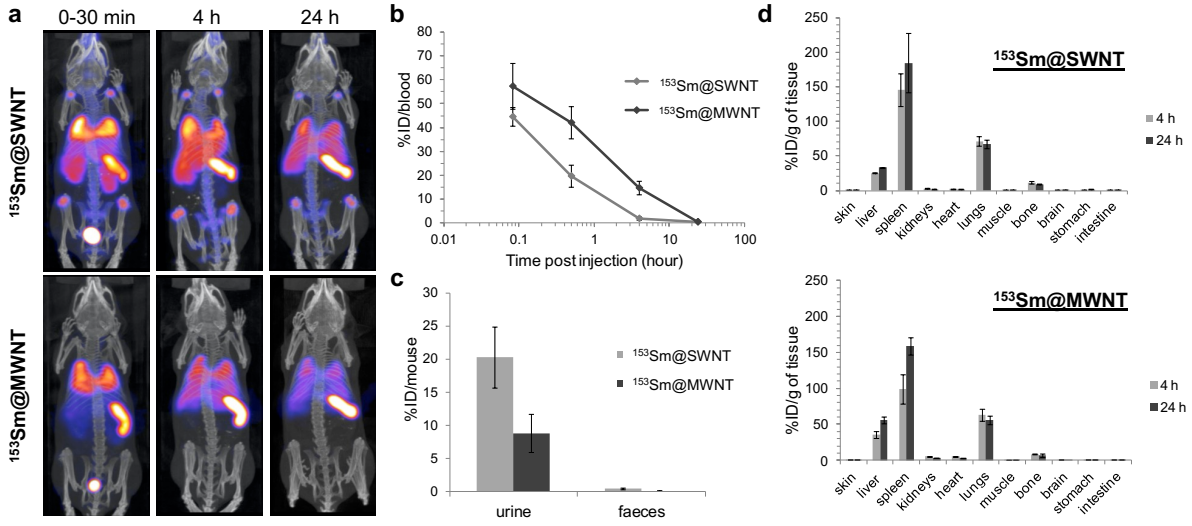

Figure 2. Whole body SPECT/CT imaging and tissue biodistribution of ^{153}Sm@SWNT and ^{153}Sm@MWNT in mice up to 24 h. a) SPECT/CT imaging, b) blood circulation, c) excretion profiles and d) tissue biodistribution profiles. C57BL/6 mice were i.v. injected with 200 μg of EDTA-quenched ^{153}Sm@SWNT or ^{153}Sm@MWNT containing 10 MBq or ~1 MBq for SPECT/CT imaging or γ-scintigraphy, respectively. In excretion studies, mice were housed individually in metabolic cages for 24 h immediately after injection. The radioactivity in blood, major organs sampled at specified time points and urine/feces collected at 24 h post injection, was measured by γ-scintigraphy. The results are expressed as mean ± S.D. (n=3-4).

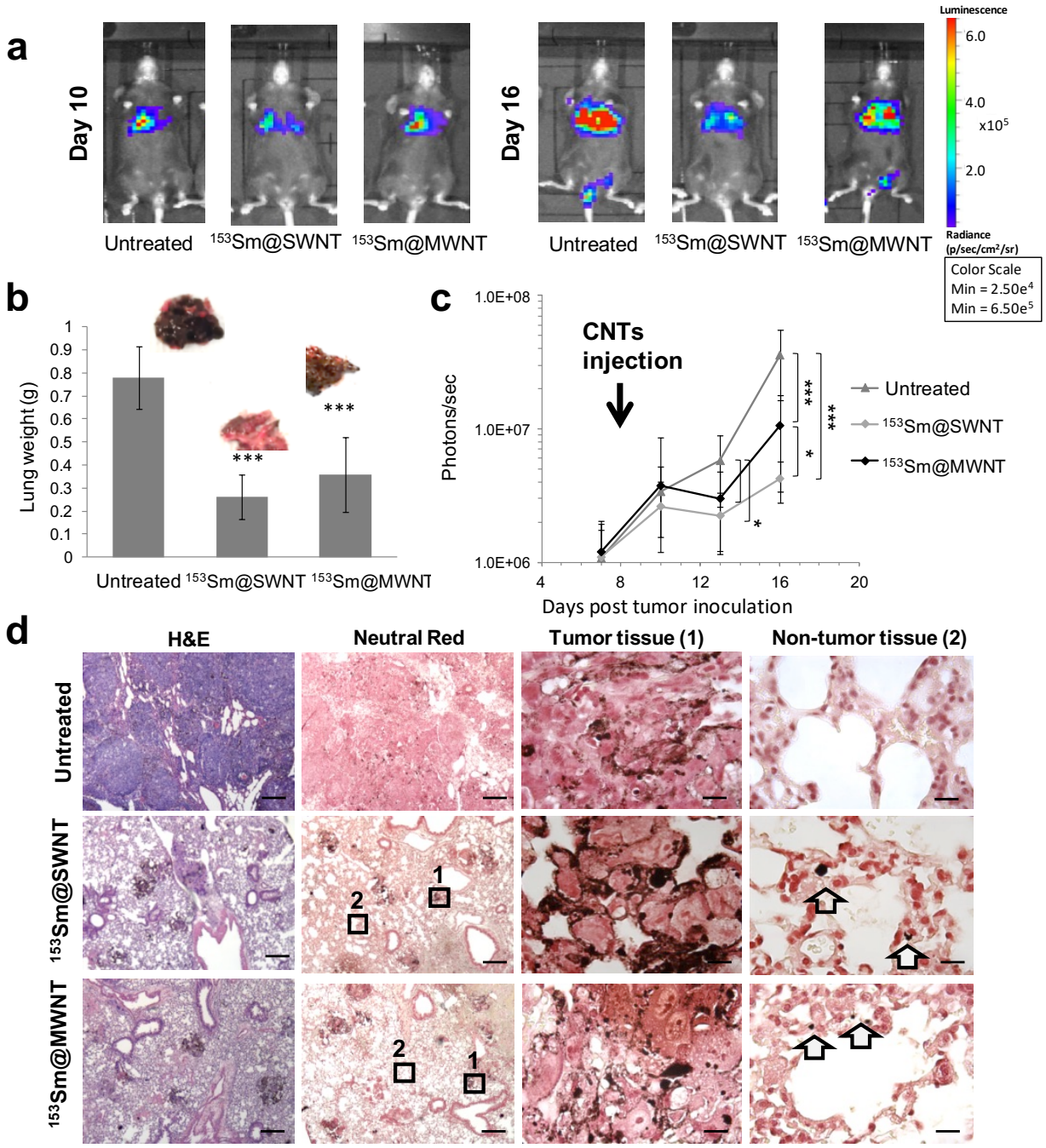

Figure 3. Tumor growth delay studies in experimental metastatic lung tumor mice model after internal administration of radiotherapy. B16F10-Luc tumor-bearing C57BL/6 mice received a single i.v. injection of ^{153}Sm@SWNT or ^{153}Sm@MWNT (20 MBq, 200 μg) on day 8 post-tumor inoculation. a) Average lung weights measured on day 16 post-tumor inoculation, the experimental

endpoint. b) Representative whole-body images of untreated, ^{153}Sm@SWNT and ^{153}Sm@MWNT treated mice captured on days 10 and 16 post-tumor inoculation. c) Tumor growth monitoring over time. Bioluminescence signals correspond to luciferase expressing B16F10 cells in the lung. d) H&E and Neutral Red stained B16F10-Luc tumor-containing lung tissue sections excised on day 16 (left panels). High magnification images of tumor (areas 1) and non-tumor (areas 2) lung tissues are shown on the right. Arrows indicate the presence of CNTs. Scale bars: 200 μm for H&E and Neutral Red stained sections; 5 μm for zoom-in images of areas 1 and 2. Results are presented as mean ± S.D. (n=9-10). Significant differences were examined using one-way ANOVA followed by Tukey's multiple comparison test (*$p < 0.05$, **$p < 0.01$, ***$p < 0.001$).

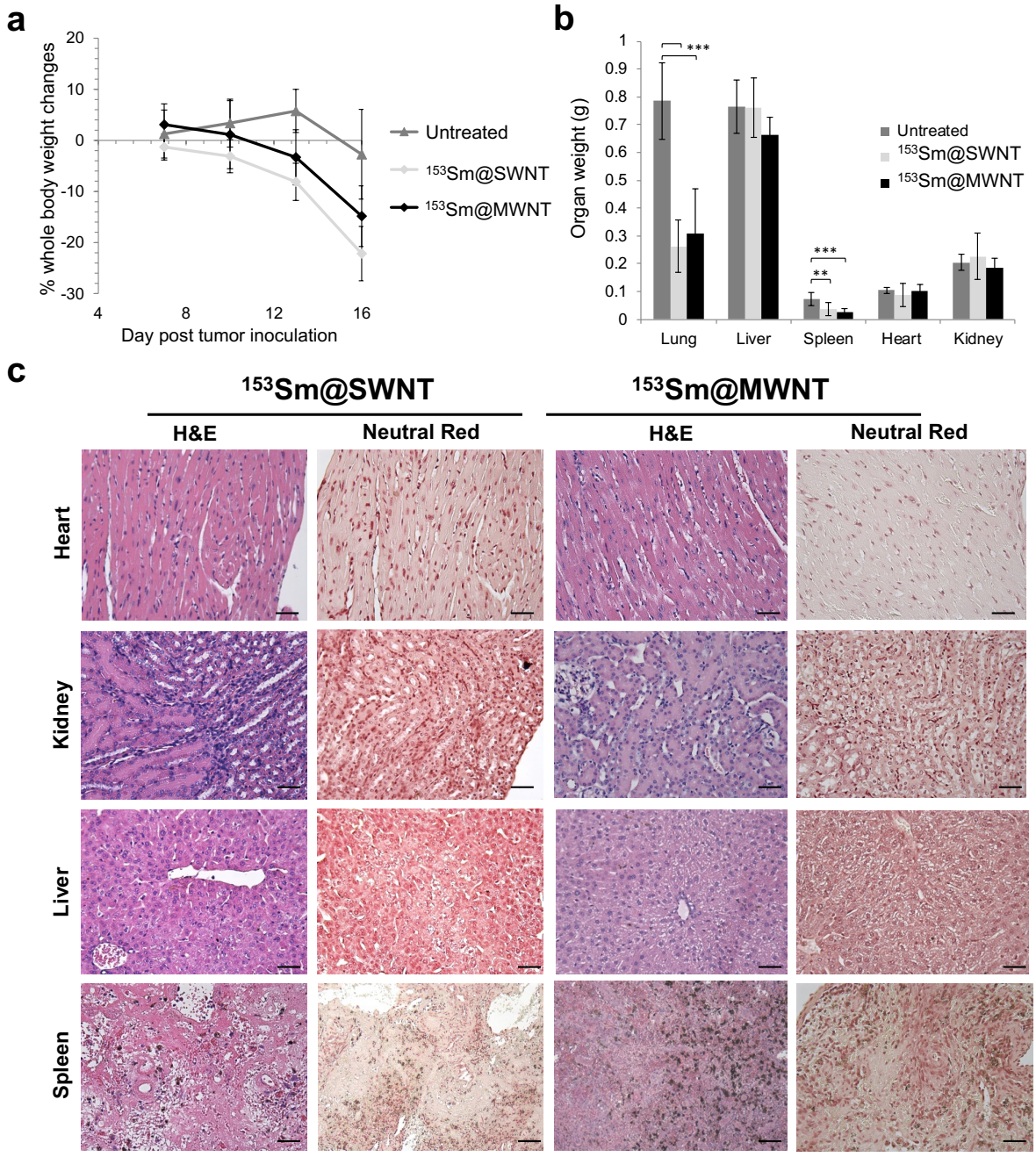

Figure 4. Toxicity assessments in tumor-bearing mice treated with ^{153}Sm@SWNT and ^{153}Sm@MWNT *via* intravenous injection. B16F10-Luc tumor-bearing C57BL/6 mice received a single i.v. injection of ^{153}Sm@SWNT or ^{153}Sm@MWNT (20 MBq, 200 μg) on day 8 post-tumor inoculation. a) Percentage of whole body weight changes of B16F10-Luc tumor-bearing mice after

radiotherapy. b) Major organ weight and c) histological examination of major organs on day 16 post tumor inoculation. The body weight of individual mouse was measured every 3-4 days post tumor-inoculation. At the experimental endpoint on day 16, major organs including heart, kidney, liver and spleen were excised, weighed and fixed for histological examination. Tissue sections were stained with H&E (examine necrosis) or Neutral Red (track CNTs). Scale bars: 50 μm. Results are presented as mean ± S.D. (n = 9-10). No statistical differences were found in % whole body weight changes between different treatments. Mice treated with ^{153}Sm@CNTs showed significant weight reduction in lung and spleen. Significant differences were examined using one-way ANOVA followed by Tukey's multiple comparison test (**$p < 0.01$, ***$p < 0.001$).

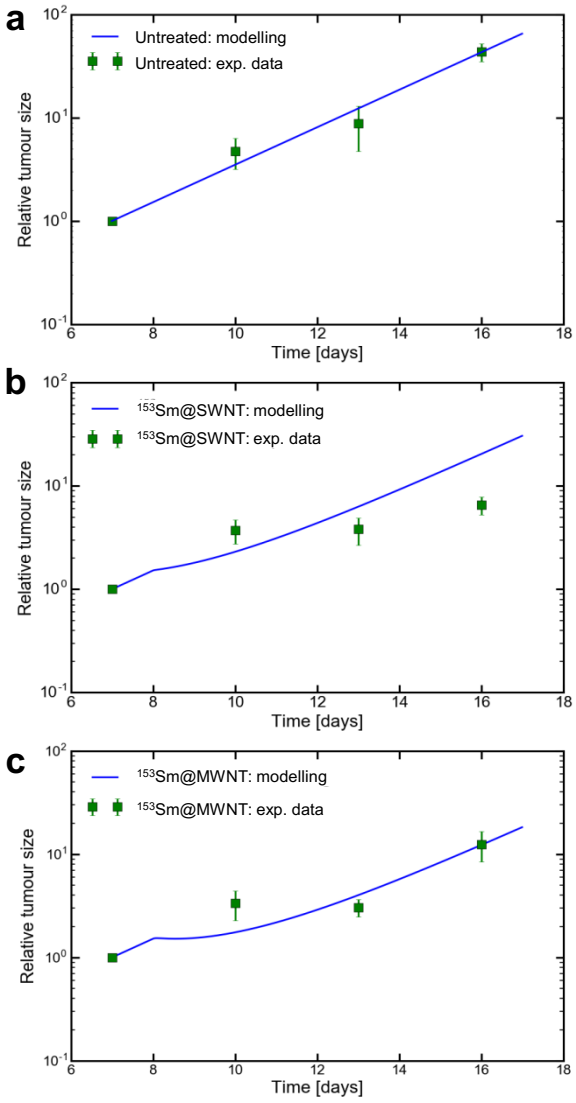

Figure 5. Predicted and experimental relative tumor sizes as a function of time in control or ^{153}Sm@SWNT- and ^{153}Sm@MWNT-treated mice. B16F10-Luc tumor-bearing C57BL/6 mice received a single dose i.v. injection of ^{153}Sm@SWNT or ^{153}Sm@MWNT (20 MBq, 200 μg) on day 8 post tumor inoculation or remained untreated. Green dots represent experiment data and blue lines are simulated results for the three groups: a) untreated control, b) ^{153}Sm@SWNT treated group, and c) ^{153}Sm@MWNT treated group. The calculated blue lines are plotted according to equation (2). The values of the coefficients entered in equation (2) are as follows: for all three

cases, the radiosensitivity parameter was α=0.0068 Gy^{-1} and the cell doubling time T_d equals 39.78 h which corresponds to a proliferation rate $\lambda = \ln(2)/T_d = 0.017\ h^{-1}$. Extrapolated initial dose rate r_0, effective uptake rate *m*, and effective washout rate *k* are specific for each case. Specifically, for the untreated sample (a), the extrapolated initial dose rate r_0 equals 0 whereas for SWNT (b) the parameter values are: $r_0 = 1.872\ Gy\ h^{-1}$, $k = 0.0162\ h^{-1}$, $m = 2.34\ h^{-1}$ and for MWNT (c) the parameter values are $r_0 = 3.158\ Gy\ h^{-1}$, $k = 0.0160\ h^{-1}$, $m = 0.826\ h^{-1}$. The detailed derivation of the parameter values for each case is given in the Dosimetry simulation section in the Supporting Information.

TABLES.

Table 1. Neutron irradiation of ^{152}Sm@SWNT and ^{152}Sm@MWNT to achieve radioactive ^{153}Sm@SWNT and ^{153}Sm@MWNT.

^{152}Sm@CNT			^{153}Sm@CNT		
Starting material	%^{152}Sm (ICP-MS)	Neutron irradiation [h]	Predicted SRA [GBq/mg]	Observed SRA [GBq/mg]	ITLC % Purity
^{152}Sm@SWNT	12.3	96	7.77	6.33	70
^{152}Sm@MWNT	17.6	96	11.11	11.37	92

ASSOCIATED CONTENT

Supporting Information.

Schematic representation employed for the development of 'hot' nanocapsules. Length distribution of ^{152}Sm @CNT samples. External diameter distribution of ^{152}Sm @CNT samples. ITLC analysis. HRTEM images of Sm-filled SWNTs before and after irradiation. Effect of the electron beam on the filling material. Table with neutron activated isotopes loaded onto nanocarriers. Tissue biodistribution of ^{153}Sm@SWNT and ^{153}Sm@MWNT. Live bioluminescence images. Live bioluminescence images of untreated mice or mice treated with ^{153}Sm@CNTs. Histological examination of major organs. Fit of the experimental biodistribution data (% ID) in the lung. Additional experimental details. This material is available free of charge *via* the Internet at http://pubs.acs.org.

AUTHOR INFORMATION

Corresponding Author

*E-mail: gerard.tobias@icmab.es (G. Tobias), khuloud.al-jamal@kcl.ac.uk (K.T. Al-Jamal), belen.ballesteros@icn2.cat (B. Ballesteros).

Author Contributions

The manuscript was written through contributions of all authors. All authors have given approval to the final version of the manuscript.

ACKNOWLEDGMENT

This work received funding from the European Union's Seventh Framework Programme (FP7-ITN Marie-Curie Actions, RADDEL, 290023). K.T. Al-Jamal acknowledges funding from

Worldwide Cancer Research (12-1054), M. Kalbac from MEYS (LL1301 and LTC18039) and G. Tobias from Agaur (2017 SGR 581). ICMAB and ICN2 acknowledge financial support from the Spanish Ministry of Economy and Competitiveness, through the "Severo Ochoa" Programme for Centres of Excellence in R&D (SEV-2015-0496 and SEV-2017-0706). This work was partly supported by the Centre National de la Recherche Scientifique (CNRS), by the Agence Nationale de la Recherche (ANR) through the LabEx project Chemistry of Complex Systems (ANR-10-LABX-0026_CSC) and by the International Center for Frontier Research in Chemistry (icFRC). We thank Thomas Swan Co. Ltd. for supplying CNT Elicarb® samples. We are grateful to S. Sandoval (ICMAB) and C. Ramos (IQS-ICMAB) for assessing the length and diameter distribution of CNTs.

REFERENCES

1. Hartshorn, C. M.; Bradbury, M. S.; Lanza, G. M.; Nel, A. E.; Rao, J.; Wang, A. Z.; Wiesner, U. B.; Yang, L.; Grodzinski, P. Nanotechnology Strategies to Advance Outcomes in Clinical Cancer Care. *ACS Nano* **2018**, *12*, 24-43.

2. Jin, Q.; Deng, Y.; Chen, X.; Ji, J. Rational Design of Cancer Nanomedicine for Simultaneous Stealth Surface and Enhanced Cellular Uptake. *ACS Nano* **2019**, *13*, 954-977.

3. Rodríguez-Nogales, C.; González-Fernández, Y.; Aldaz, A.; Couvreur, P.; Blanco-Prieto, M. J. Nanomedicines for Pediatric Cancers. *ACS Nano* **2018**, *12*, 7482-7496.

4. Björnmalm, M.; Thurecht, K. J.; Michael, M.; Scott, A. M.; Caruso, F. Bridging Bio–Nano Science and Cancer Nanomedicine. *ACS Nano* **2017**, *11*, 9594-9613.

5. Liu, Z.; Jiang, W.; Nam, J.; Moon, J. J.; Kim, B. Y. S. Immunomodulating Nanomedicine for Cancer Therapy. *Nano Lett.* **2018**, *18*, 6655-6659.

6. Hong, G.; Diao, S.; Antaris, A. L.; Dai, H. Carbon Nanomaterials for Biological Imaging and Nanomedicinal Therapy. *Chem. Rev.* **2015**, *115*, 10816-10906.

7. Serpell, C. J.; Kostarelos, K.; Davis, B. G. Can Carbon Nanotubes Deliver on Their Promise in Biology? Harnessing Unique Properties for Unparalleled Applications. *ACS Central Sci.* **2016**, *2*, 190-200.

8. Hernández-Rivera, M.; Zaibaq, N. G.; Wilson, L. J. Toward Carbon Nanotube-Based Imaging Agents for the Clinic. *Biomaterials* **2016**, *101*, 229-240.

9. Loh, K. P.; Ho, D.; Chiu, G. N. C.; Leong, D. T.; Pastorin, G.; Chow, E. K.-H. Clinical Applications of Carbon Nanomaterials in Diagnostics and Therapy. *Adv. Mater.* **2018**, *30*, 1802368.

10. Calatayud, D. G.; Ge, H.; Kuganathan, N.; Mirabello, V.; Jacobs, R. M. J.; Rees, N. H.; Stoppiello, C. T.; Khlobystov, A. N.; Tyrrell, R. M.; Como, E. D.; Pascu, S. I. Encapsulation of Cadmium Selenide Nanocrystals in Biocompatible Nanotubes: DFT Calculations, X-Ray Diffraction Investigations, and Confocal Fluorescence Imaging. *ChemistryOpen* **2018**, *7*, 144-158.

11. Al-Jamal, K. T.; Nerl, H.; Muller, K. H.; Ali-Boucetta, H.; Li, S. P.; Haynes, P. D.; Jinschek, J. R.; Prato, M.; Bianco, A.; Kostarelos, K.; Porter, A. E. Cellular Uptake Mechanisms of Functionalised Multi-Walled Carbon Nanotubes by 3d Electron Tomography Imaging. *Nanoscale* **2011**, *3*, 2627-2635.

12. Kafa, H.; Wang, J. T.-W.; Rubio, N.; Venner, K.; Anderson, G.; Pach, E.; Ballesteros, B.; Preston, J. E.; Abbott, N. J.; Al-Jamal, K. T. The Interaction of Carbon Nanotubes with an *In Vitro* Blood-Brain Barrier Model and Mouse Brain *In Vivo*. *Biomaterials* **2015**, *53*, 437-452.

13. Pantarotto, D.; Singh, R.; McCarthy, D.; Erhardt, M.; Briand, J. P.; Prato, M.; Kostarelos, K.; Bianco, A. Functionalized Carbon Nanotubes for Plasmid DNA Gene Delivery. *Angew. Chem. Int. Ed.* **2004**, *43*, 5242-5246.

14. Pantarotto, D.; Singh, R.; McCarthy, D.; Erhardt, M.; Briand, J.-P.; Prato, M.; Kostarelos, K.; Bianco, A. Functionalized Carbon Nanotubes for Plasmid DNA Gene Delivery. *Angew. Chem. Int. Ed.* **2004**, *116*, 5354-5358.

15. Battigelli, A.; Ménard-Moyon, C.; Da Ros, T.; Prato, M.; Bianco, A. Endowing Carbon Nanotubes with Biological and Biomedical Properties by Chemical Modifications. *Adv. Drug Deliv. Rev.* **2013**, *65*, 1899-1920.

16. Dinesh, B.; Bianco, A.; Ménard-Moyon, C. Designing Multimodal Carbon Nanotubes by Covalent Multi-Functionalization. *Nanoscale* **2016**, *8*, 18596-18611.

17. Marega, R.; Bonifazi, D. Filling Carbon Nanotubes for Nanobiotechnological Applications. *New J. Chem.* **2014**, *38*, 22-27.

18. Heister, E.; Brunner, E. W.; Dieckmann, G. R.; Jurewicz, I.; Dalton, A. B. Are Carbon Nanotubes a Natural Solution? Applications in Biology and Medicine. *ACS Appl. Mater. Interfaces* **2013**, *5*, 1870-1891.

19. Kotchey, G. P.; Hasan, S. A.; Kapralov, A. A.; Ha, S. H.; Kim, K.; Shvedova, A. A.; Kagan, V. E.; Star, A. A Natural Vanishing Act: The Enzyme-Catalyzed Degradation of Carbon Nanomaterials. *Acc. Chem. Res.* **2012**, *45*, 1770-1781.

20. Ueda, M.; Seo, S.; Nair, B. G.; Müller, S.; Takahashi, E.; Arai, T.; Iyoda, T.; Fujii, S.-i.; Tsuneda, S.; Ito, Y. End-Sealed High Aspect Ratio Hollow Nanotubes Encapsulating an Anticancer Drug: Torpedo-Shaped Peptidic Nanocapsules. *ACS Nano* **2019**, *13*, 305-312.

21. Chen, X.; Zhang, Q.; Li, J.; Yang, M.; Zhao, N.; Xu, F.-J. Rattle-Structured Rough Nanocapsules with *In-Situ*-Formed Gold Nanorod Cores for Complementary Gene/Chemo/Photothermal Therapy. *ACS Nano* **2018**, *12*, 5646-5656.

22. Ijäs, H.; Hakaste, I.; Shen, B.; Kostiainen, M. A.; Linko, V. Reconfigurable DNA Origami Nanocapsule for Ph-Controlled Encapsulation and Display of Cargo. *ACS Nano* **2019**, *13*, 5959-5967.

23. Wang, S.; Liu, X.; Chen, S.; Liu, Z.; Zhang, X.; Liang, X.-J.; Li, L. Regulation of Ca^{2+} Signaling for Drug-Resistant Breast Cancer Therapy with Mesoporous Silica Nanocapsule Encapsulated Doxorubicin/Sirna Cocktail. *ACS Nano* **2019**, *13*, 274-283.

24. González-Aramundiz, J. V.; Peleteiro, M.; González-Fernández, Á.; Alonso, M. J.; Csaba, N. S. Protamine Nanocapsules for the Development of Thermostable Adjuvanted Nanovaccines. *Mol. Pharm.* **2018**, *15*, 5653-5664.

25. Hong, S. Y.; Tobias, G.; Al-Jamal, K. T.; Ballesteros, B.; Ali-Boucetta, H.; Lozano-Perez, S.; Nellist, P. D.; Sim, R. B.; Finucane, C.; Mather, S. J.; Green, M. L. H.; Kostarelos, K.; Davis, B. G. Filled and Glycosylated Carbon Nanotubes for *In Viv*o Radioemitter Localization and Imaging. *Nat. Mater.* **2010**, *9*, 485-490.

26. Strano, M. S. Nanoscale Radiosurgery. *Nat. Mater.* **2010**, *9*, 467.

27. Ge, H.; Riss, P. J.; Mirabello, V.; Calatayud, D. G.; Flower, S. E.; Arrowsmith, R. L.; Fryer, T. D.; Hong, Y.; Sawiak, S.; Jacobs, R. M. J.; Botchway, S. W.; Tyrrell, R. M.; James, T. D.; Fossey, J. S.; Dilworth, J. R.; Aigbirhio, F. I.; Pascu, S. I. Behavior of Supramolecular Assemblies of Radiometal-Filled and Fluorescent Carbon Nanocapsules *In Vitro* and *In Vivo*. *Chem* **2017**, *3*, 437-460.

28. De Munari, S.; Sandoval, S.; Pach, E.; Ballesteros, B.; Tobias, G.; Anthony, D. C.; Davis, B. G. *In Vivo* Behaviour of Glyco-NaI@SWCNT 'Nanobottles'. *Inorg. Chim. Acta* **2019**, *495*, 118933.

29. Shao, L.; Tobias, G.; Huh, Y.; Green, M. L. H. Reversible Filling of Single Walled Carbon Nanotubes Opened by Alkali Hydroxides. *Carbon* **2006**, *44*, 2855-2858.

30. Martincic, M.; Vranic, S.; Pach, E.; Ballesteros, B.; Kostarelos, K.; Tobias, G. Non-Cytotoxic Carbon Nanocapsules Synthesized *via* One-Pot Filling and End-Closing of Multi-Walled Carbon Nanotubes. *Carbon* **2019**, *141*, 782-793.

31. Kierkowicz, M.; González-Domínguez, J. M.; Pach, E.; Sandoval, S.; Ballesteros, B.; Da Ros, T.; Tobias, G. Filling Single-Walled Carbon Nanotubes with Lutetium Chloride: A Sustainable Production of Nanocapsules Free of Nonencapsulated Material. *ACS Sustain. Chem. Eng.* **2017**, *5*, 2501-2508.

32. Serpell, C. J.; Rutte, R. N.; Geraki, K.; Pach, E.; Martincic, M.; Kierkowicz, M.; De Munari, S.; Wals, K.; Raj, R.; Ballesteros, B.; Tobias, G.; Anthony, D. C.; Davis, B. G. Carbon Nanotubes Allow Capture of Krypton, Barium and Lead for Multichannel Biological X-Ray Fluorescence Imaging. *Nat. Commun.* **2016**, *7*, 13118.

33. Song, G.; Cheng, L.; Chao, Y.; Yang, K.; Liu, Z. Emerging Nanotechnology and Advanced Materials for Cancer Radiation Therapy. *Adv. Mater.* **2017**, *29*, 1700996.

34. Goel, S.; England, C. G.; Chen, F.; Cai, W. Positron Emission Tomography and Nanotechnology: A Dynamic Duo for Cancer Theranostics. *Adv. Drug Deliv. Rev.* **2017**, *113*, 157-176.

35. Kunz-Schughart, L. A.; Dubrovska, A.; Peitzsch, C.; Ewe, A.; Aigner, A.; Schellenburg, S.; Muders, M. H.; Hampel, S.; Cirillo, G.; Iemma, F.; Tietze, R.; Alexiou, C.; Stephan, H.;

Zarschler, K.; Vittorio, O.; Kavallaris, M.; Parak, W. J.; Mädler, L.; Pokhrel, S. Nanoparticles for Radiooncology: Mission, Vision, Challenges. *Biomaterials* **2017**, *120*, 155-184.

36. Ehlerding, E. B.; Grodzinski, P.; Cai, W.; Liu, C. H. Big Potential from Small Agents: Nanoparticles for Imaging-Based Companion Diagnostics. *ACS Nano* **2018**, *12*, 2106-2121.

37. Singh, R.; Pantarotto, D.; Lacerda, L.; Pastorin, G.; Klumpp, C.; Prato, M.; Bianco, A.; Kostarelos, K. Tissue Biodistribution and Blood Clearance Rates of Intravenously Administered Carbon Nanotube Radiotracers. *Proc. Natl. Acad. Sci. U. S. A.* **2006**, *103*, 3357-3362.

38. McDevitt, M. R.; Chattopadhyay, D.; Jaggi, J. S.; Finn, R. D.; Zanzonico, P. B.; Villa, C.; Rey, D.; Mendenhall, J.; Batt, C. A.; Njardarson, J. T.; Scheinberg, D. A. Pet Imaging of Soluble Yttrium-86-Labeled Carbon Nanotubes in Mice. *PLoS ONE* **2007**, *2*, e907.

39. Ruggiero, A.; Villa, C. H.; Holland, J. P.; Sprinkle, S. R.; May, C.; Lewis, J. S.; Scheinberg, D. A.; McDevitt, M. R. Imaging and Treating Tumor Vasculature with Targeted Radiolabeled Carbon Nanotubes. *Int. J. Nanomed.* **2010**, *5*, 783-802.

40. Hartman, K. B.; Hamlin, D. K.; Wilbur, D. S.; Wilson, L. J. ^{211}AtCl@US-Tube Nanocapsules: A New Concept in Radiotherapeutic-Agent Design. *Small* **2007**, *3*, 1496-1499.

41. Cisneros, B. T.; Law, J. J.; Matson, M. L.; Azhdarinia, A.; Sevick-Muraca, E. M.; Wilson, L. J. Stable Confinement of Positron Emission Tomography and Magnetic Resonance Agents within Carbon Nanotubes for Bimodal Imaging. *Nanomedicine* **2014**, *9*, 2499-2509.

42. Matson, M. L.; Villa, C. H.; Ananta, J. S.; Law, J. J.; Scheinberg, D. A.; Wilson, L. J. Encapsulation of Alpha-Particle-Emitting $^{225}Ac^{3+}$ Ions within Carbon Nanotubes. *J. Nucl. Med.* **2015**, *56*, 897-900.

43. Ren, Y.; Pastorin, G. Incorporation of Hexamethylmelamine inside Capped Carbon Nanotubes. *Adv. Mater.* **2008**, *20*, 2031-2036.

44. Shao, L.; Lin, T.-W.; Tobias, G.; Green, M. L. H. A Simple Method for the Containment and Purification of Filled Open-Ended Single Wall Carbon Nanotubes Using C_{60} Molecules. *Chem. Commun*. **2008**, 2164-2166.

45. Bayouth, J. E.; Macey, D. J.; Kasi, L. P.; Fossella, F. V. Dosimetry and Toxicity of Samarium-153-EDTMP Administered for Bone Pain Due to Skeletal Metastases. *J. Nucl. Med*. **1994**, *35*, 63-9.

46. Yeong, C.-H.; Abdullah, B. J. J.; Ng, K.-H.; Chung, L.-Y.; Goh, K.-L.; Sarji, S. A.; Perkins, A. C. Production and First Use of $^{153}SmCl_3$-Ion Exchange Resin Capsule Formulation for Assessing Gastrointestinal Motility. *Appl. Radiat. Isot*. **2012**, *70*, 450-455.

47. Anderson, P. Samarium for Osteoblastic Bone Metastases and Osteosarcoma. *Expert Opin. Pharmacother*. **2006**, *7*, 1475-86.

48. Hashikin, N. A.; Yeong, C. H.; Abdullah, B. J.; Ng, K. H.; Chung, L. Y.; Dahalan, R.; Perkins, A. C. Neutron Activated Samarium-153 Microparticles for Transarterial Radioembolization of Liver Tumour with Post-Procedure Imaging Capabilities. *PLoS One* **2015**, *10*, e0138106.

49. Hamoudeh, M.; Fessi, H.; Salim, H.; Barbos, D. Holmium-Loaded PLLA Nanoparticles for Intratumoral Radiotherapy *via* the TMT Technique: Preparation, Characterization, and Stability Evaluation after Neutron Irradiation. *Drug Dev. Ind. Pharm*. **2008**, *34*, 796-806.

50. Bult, W.; Varkevisser, R.; Soulimani, F.; Seevinck, P. R.; de Leeuw, H.; Bakker, C. J. G.; Luijten, P. R.; van het Schip, A. D.; Hennink, W. E.; Nijsen, J. F. W. Holmium Nanoparticles: Preparation and *In Vitro* Characterization of a New Device for Radioablation of Solid Malignancies. *Pharm. Res*. **2010**, *27*, 2205-2212.

51. Di Pasqua, A. J.; Huckle, J. E.; Kim, J.-K.; Chung, Y.; Wang, A. Z.; Jay, M.; Lu, X. Preparation of Neutron-Activatable Holmium Nanoparticles for the Treatment of Ovarian Cancer Metastases. *Small* **2012**, *8*, 997-1000.

52. Cagle, D. W.; Thrash, T. P.; Alford, M.; Chibante, L. P. F.; Ehrhardt, G. J.; Wilson, L. J. Synthesis, Characterization, and Neutron Activation of Holmium Metallofullerenes. *J. Am. Chem. Soc.* **1996**, *118*, 8043-8047.

53. Cagle, D. W.; Kennel, S. J.; Mirzadeh, S.; Alford, J. M.; Wilson, L. J. *In Vivo* Studies of Fullerene-Based Materials Using Endohedral Metallofullerene Radiotracers. *Proc. Natl. Acad. Sci. U. S. A.* **1999**, *96*, 5182-5187.

54. Di Pasqua, A. J.; Yuan, H.; Chung, Y.; Kim, J. K.; Huckle, J. E.; Li, C.; Sadgrove, M.; Tran, T. H.; Jay, M.; Lu, X. Neutron-Activatable Holmium-Containing Mesoporous Silica Nanoparticles as a Potential Radionuclide Therapeutic Agent for Ovarian Cancer. *J. Nucl. Med.* **2013**, *54*, 111-116.

55. Di Pasqua, A. J.; Miller, M. L.; Lu, X.; Peng, L.; Jay, M. Tumor Accumulation of Neutron-Activatable Holmium-Containing Mesoporous Silica Nanoparticles in an Orthotopic Non-Small Cell Lung Cancer Mouse Model. *Inorg. Chim. Acta* **2012**, *393*, 334-336.

56. Munaweera, I.; Koneru, B.; Shi, Y.; Pasqua, A. J. D.; Kenneth J. Balkus, J. Chemoradiotherapeutic Wrinkled Mesoporous Silica Nanoparticles for Use in Cancer Therapy. *APL Mater.* **2014**, *2*, 113315.

57. Munaweera, I.; Shi, Y.; Koneru, B.; Saez, R.; Aliev, A.; Di Pasqua, A. J.; Balkus, K. J. Chemoradiotherapeutic Magnetic Nanoparticles for Targeted Treatment of Nonsmall Cell Lung Cancer. *Mol. Pharm.* **2015**, *12*, 3588-3596.

58. Kim, J.; Luo, Z.-X.; Wu, Y.; Lu, X.; Jay, M. *In-Situ* Formation of Holmium Oxide in Pores of Mesoporous Carbon Nanoparticles as Substrates for Neutron-Activatable Radiotherapeutics. *Carbon* **2017**, *117*, 92-99.

59. Kim, J.; Jay, M. Neutron-Activatable Radionuclide Cancer Therapy Using Graphene Oxide Nanoplatelets. *Nucl. Med. Biol.* **2017**, *52*, 42-48.

60. Smits, M. L. J.; Nijsen, J. F. W.; van den Bosch, M. A. A. J.; Lam, M. G. E. H.; Vente, M. A. D.; Mali, W. P. T. M.; van het Schip, A. D.; Zonnenberg, B. A. Holmium-166 Radioembolisation in Patients with Unresectable, Chemorefractory Liver Metastases (HEPAR Trial): A Phase 1, Dose-Escalation Study. *Lancet Oncol.* **2012**, *13*, 1025-1034.

61. Radosa, C. G.; Radosa, J. C.; Grosche-Schlee, S.; Zöphel, K.; Plodeck, V.; Kühn, J. P.; Kotzerke, J.; Hoffmann, R.-T. Holmium-166 Radioembolization in Hepatocellular Carcinoma: Feasibility and Safety of a New Treatment Option in Clinical Practice. *Cardiovasc. Interv. Radiol.* **2019**, *42*, 405-412.

62. Kierkowicz, M.; Pach, E.; Santidrián, A.; Sandoval, S.; Gonçalves, G.; Tobías-Rossell, E.; Kalbáč, M.; Ballesteros, B.; Tobias, G. Comparative Study of Shortening and Cutting Strategies of Single-Walled and Multi-Walled Carbon Nanotubes Assessed by Scanning Electron Microscopy. *Carbon* **2018**, *139*, 922-932.

63. *Manual for Reactor Produced Radioisotopes, Iaea-Tecdoc-1340*. Vienna, Austria, **2003**, 189-192.

64. Giulio, C.; Simonelli, F.; Holzwarth, U.; Gibson, P. Neutron Activation of Nanoparticles. In *Isotopes in Nanoparticles: Fundamentals and Applications*; Llop-Roig, J., Gómez-Vallejo, V., Gibson, N., Eds.; Pan Stanford Publishing: Boca Raton, 2016; pp 315-334.

65. Martincic, M.; Pach, E.; Ballesteros, B.; Tobias, G. Quantitative Monitoring of the Removal of Non-Encapsulated Material External to Filled Carbon Nanotube Samples. *Phys. Chem. Chem. Phys.* **2015**, *17*, 31662-31669.

66. Hutchison, J. L.; Grobert, N.; Zakalyukin, R. M.; Eliseev, A. A.; Chernisheva, M. V.; Kumskov, A. S.; Grigoriev, Y. V.; Krestinin, A. V.; Freitag, B.; Kiselev, N. A. The Behaviour of 1D CuI Crystal@SWNT Nanocomposite under Electron Irradiation. *AIP Conf. Proc.* **2008**, *999*, 79-92.

67. Cabana, L.; Ballesteros, B.; Batista, E.; Magén, C.; Arenal, R.; Oró-Solé, J.; Rurali, R.; Tobias, G. Synthesis of PbI_2 Single-Layered Inorganic Nanotubes Encapsulated within Carbon Nanotubes. *Adv. Mater.* **2014**, *26*, 2016-2021.

68. Hart, M.; White, E. R.; Chen, J.; McGilvery, C. M.; Pickard, C. J.; Michaelides, A.; Sella, A.; Shaffer, M. S. P.; Salzmann, C. G. Encapsulation and Polymerization of White Phosphorus inside Single-Wall Carbon Nanotubes. *Angew. Chem. Int. Ed.* **2017**, *56*, 8144-8148.

69. Sandoval, S.; Kepić, D.; Pérez del Pino, Á.; György, E.; Gómez, A.; Pfannmoeller, M.; Tendeloo, G. V.; Ballesteros, B.; Tobias, G. Selective Laser-Assisted Synthesis of Tubular van der Waals Heterostructures of Single-Layered PbI_2 within Carbon Nanotubes Exhibiting Carrier Photogeneration. *ACS Nano* **2018**, *12*, 6648-6656.

70. Vasylenko, A.; Marks, S.; Wynn, J. M.; Medeiros, P. V. C.; Ramasse, Q. M.; Morris, A. J.; Sloan, J.; Quigley, D. Electronic Structure Control of Sub-Nanometer 1D SnTe *via* Nanostructuring within Single-Walled Carbon Nanotubes. *ACS Nano* **2018**, *12*, 6023-6031.

71. Slade, C. A.; Sanchez, A. M.; Sloan, J. Unprecedented New Crystalline Forms of SnSe in Narrow to Medium Diameter Carbon Nanotubes. *Nano Lett.* **2019**, *19*, 2979-2984.

72. Tse, J. W.; Wiebe, L. I.; Noujaim, A. A. High Specific Activity [Samarium-153] EDTA for Imaging of Experimental Tumor Models. *J. Nucl. Med.* **1989**, *30*, 202-208.

73. Fidler, I. J. Selection of Successive Tumour Lines for Metastasis. *Nat. New Biol.* **1973**, *242*, 148-149.

74. Siddikuzzaman; Grace, V. M. B. Inhibition of Metastatic Lung Cancer in C57BL/6 Mice by Liposome Encapsulated All Trans Retinoic Acid (ATRA). *Int. Immunopharmacol.* **2012**, *14*, 570-579.

75. Perez Ruiz de Garibay, A.; Spinato, C.; Klippstein, R.; Bourgognon, M.; Martincic, M.; Pach, E.; Ballesteros, B.; Ménard-Moyon, C.; Al-Jamal, K. T.; Tobias, G.; Bianco, A. Evaluation of the Immunological Profile of Antibody-Functionalized Metal-Filled Single-Walled Carbon Nanocapsules for Targeted Radiotherapy. *Sci. Rep.* **2017**, *7*, 42605.

76. Kallini, J. R.; Gabr, A.; Thorlund, K.; Balijepalli, C.; Ayres, D.; Kanters, S.; Ebrahim, S.; Mills, E.; Lewandowski, R. J.; Salem, R. Comparison of the Adverse Event Profile of Therasphere® with SIR-Spheres® for the Treatment of Unresectable Hepatocellular Carcinoma: A Systematic Review. *Cardiovasc. Interv. Radiol.* **2017**, *40*, 1033-1043.

77. TheraSphere®. [Package Insert]. Biocompatibles UK Ltd., Surrey, 2014.

78. SIR-Spheres®. [Package Insert]. Sirtex Medical Limited, North Sydney, 2014.

79. TheraSphere®. [FDA Humanitarian Device Exemption: H980006 Summary of safety and portable benefit]. Biocompatibles UK Ltd., Surrey, 1999.

80. Martincic, M.; Frontera, C.; Pach, E.; Ballesteros, B.; Tobias, G. Synthesis of Dry $SmCl_3$ from Sm_2O_3 Revisited. Implications for the Encapsulation of Samarium Compounds into Carbon Nanotubes. *Polyhedron* **2016**, *116*, 116-121.

81. Sandoval, S.; Kierkowicz, M.; Pach, E.; Ballesteros, B.; Tobias, G. Determination of the Length of Single-Walled Carbon Nanotubes by Scanning Electron Microscopy. *MethodsX* **2018**, *5*, 1465-1472.

82. Šefl, M.; Kyriakou, I.; Emfietzoglou, D. Technical Note: Impact of Cell Repopulation and Radionuclide Uptake Phase on Cell Survival. *Med. Phys.* **2016**, *43*, 2715-2720.

83. Stabin, M. G.; Konijnenberg, M. W. Re-Evaluation of Absorbed Fractions for Photons and Electrons in Spheres of Various Sizes. *J. Nucl. Med.* **2000**, *41*, 149-160.

84. Schiller, U.; Hoffmann, W.; Bamberg, M.; Rodemann, H. P. All-Trans-Retinoic Acid Modulates the Radiosensitivity of Proliferating Cells. *Int. J. Cancer* **1997**, *70*, 488-490.

85. Chapman, J. D.; Nahum, A. E. *Radiotherapy Treatment Planning: Linear-Quadratic Radiobiology*; CRC Press, Taylor & Francis Group: Boca Raton, 2015.

86. Dale, R. G. Dose-Rate Effects in Targeted Radiotherapy. *Phys. Med. Biol.* **1996**, *41*, 1871-1884.

TABLE OF CONTENTS

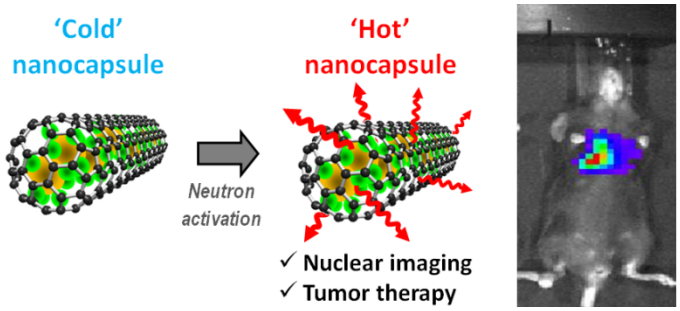

- Supporting Information -

Neutron Activated ^{153}Sm Sealed in Carbon Nanocapsules for *In Vivo* Imaging and Tumor Radiotherapy

Julie T.-W. Wang[a], Rebecca Klippstein[a], Markus Martincic[b], Elzbieta Pach[c], Robert Feldman[d], Martin Šefl[e,f], Yves Michel[d], Daniel Asker[a], Jane K. Sosabowski[g], Martin Kalbac[h], Tatiana Da Ros[i], Cécilia Ménard-Moyon[j], Alberto Bianco[j], Ioanna Kyriakou[e], Dimitris Emfietzoglou[e], Jean-Claude Saccavini[d], Belén Ballesteros[c,], Khuloud T. Al-Jamal[a,]* and Gerard Tobias[b,]**

[a]Institute of Pharmaceutical Science, King's College London, London SE1 9NH, UK

[b]Institut de Ciència de Materials de Barcelona (ICMAB-CSIC), Campus UAB, 08193 Bellaterra, Barcelona, Spain

[c]Catalan Institute of Nanoscience and Nanotechnology (ICN2), CSIC and the Barcelona Institute of Science and Technology, Campus UAB, 08193 Bellaterra, Barcelona, Spain

[d]Cis Bio International Ion Beam Applications SA, Gif sur Yvette 91192, France

[e]Medical Physics Laboratory, University of Ioannina Medical School, Ioannina GR-45110, Greece

[f]Faculty of Nuclear Sciences and Physical Engineering, Czech Technical University in Prague, Prague 11519, Czech Republic

[g]Centre for Molecular Oncology, Barts Cancer Institute, Queen Mary University of London, London EC1M 6BQ, UK

[h]J. Heyrovsky Institute of the Physical Chemistry, Dolejskova 3, 182 23 Prague 8, Czech Republic

[i]INSTM Unit of Trieste, Department of Chemical and Pharmaceutical Sciences, University of Trieste, Via L. Giorgieri 1, 34127 Trieste, Italy

[j]University of Strasbourg, CNRS, Immunology, Immunopathology and Therapeutic Chemistry, UPR 3572, 67000 Strasbourg, France.

*Corresponding authors E-mail: gerard.tobias@icmab.es, khuloud.al-jamal@kcl.ac.uk, belen.ballesteros@icn2.cat.

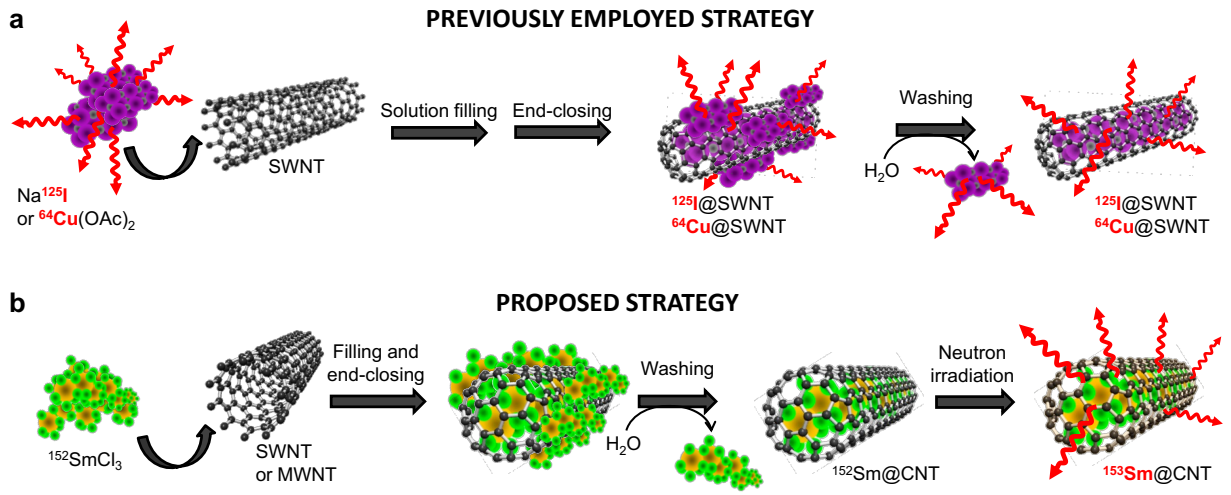

Figure S1. Schematic representation of the strategies employed for the hermetic sealing of radionuclides into the cavities of carbon nanotubes (hot nanocapsules). a) Previously employed strategies where radionuclides (^{125}I and ^{64}Cu) are directly filled into carbon nanotubes[1, 2]. b) Present strategy, also depicted in Fig. 1a (main text), where a non-radioactive enriched precursor is initially encapsulated (^{152}Sm) and it is activated into its radioactive form by neutron irradiation (^{153}Sm) in the last step. In both schematic representations, the wavy lines indicate radioactivity emerging from radionuclides (highlighted in the text in red).

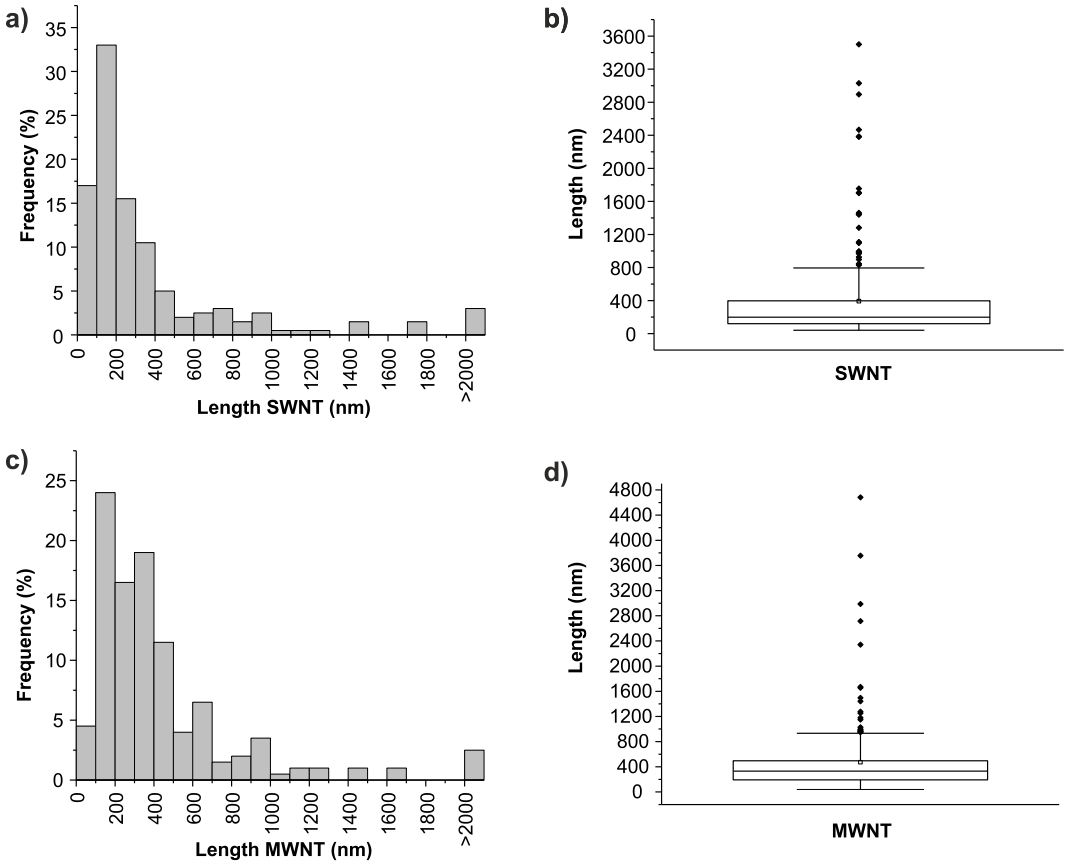

Figure S2. Length distribution of ^{152}Sm@CNT samples. a) Length distribution histogram and b) box plot analysis of SWNT; c) Length distribution histogram and d) box plot analysis of MWNT.

Table S1. Descriptive analysis of the length distribution of ^{152}Sm@CNT samples.

	N Number of measured CNT	Median (nm)	Lower observation (nm)	Lower adjacent observation (nm)	Q1 25th percentile (nm)	Q3 75th percentile (nm)	Maximum adjacent observation (nm)	Maximum observation (nm)
SWNT	200	199	41	41	120	397	794	3500
MWNT	200	331	40	40	192	495	932	4682

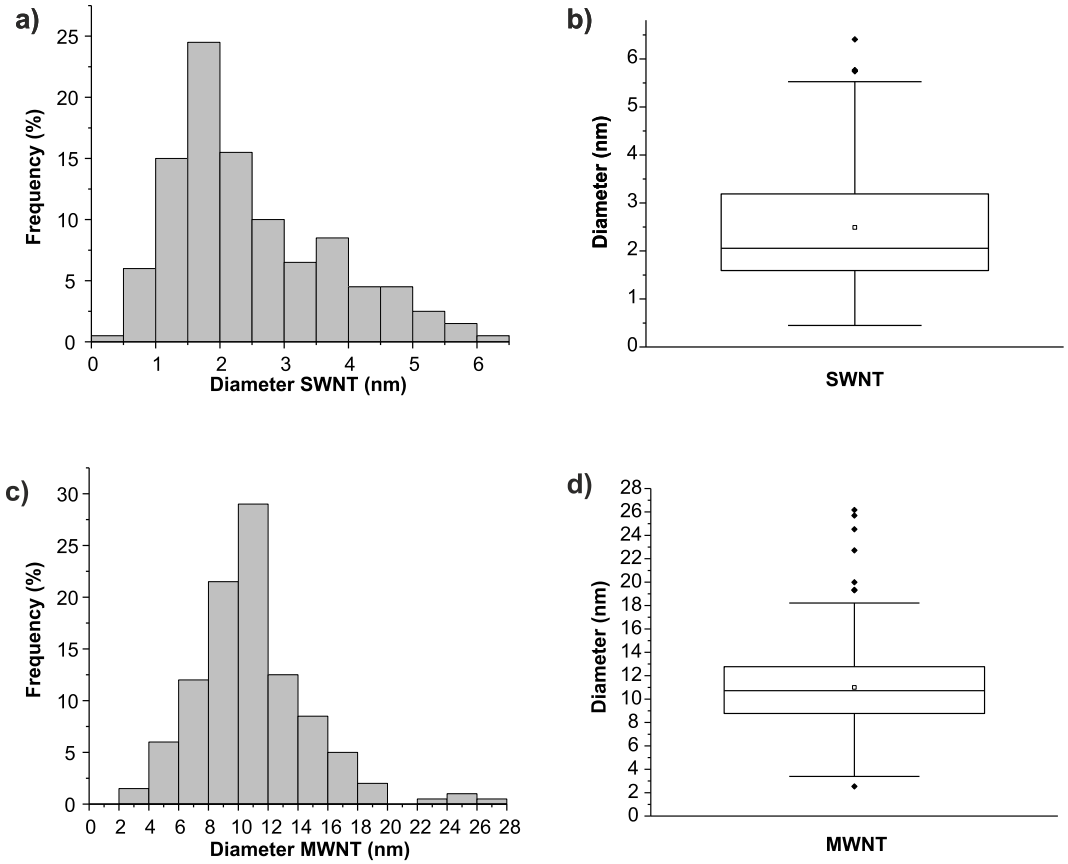

Figure S3. External diameter distribution of ^{152}Sm@CNT samples. a) Diameter distribution histogram and b) box plot analysis of SWNT; c) Diameter distribution histogram and d) box plot analysis of MWNT.

Table S2. Descriptive analysis of the external diameter distribution of ^{152}Sm@CNT samples.

	N Number of measured CNT	Median (nm)	Lower observation (nm)	Lower adjacent observation (nm)	Q1 25^{th} percentile (nm)	Q3 75^{th} percentile (nm)	Maximum adjacent observation (nm)	Maximum observation (nm)
SWNT	200	2.1	0.5	0.5	1.6	3.2	5.5	6.4
MWNT	200	10.7	2.5	3.4	8.8	12.8	18.2	26.2

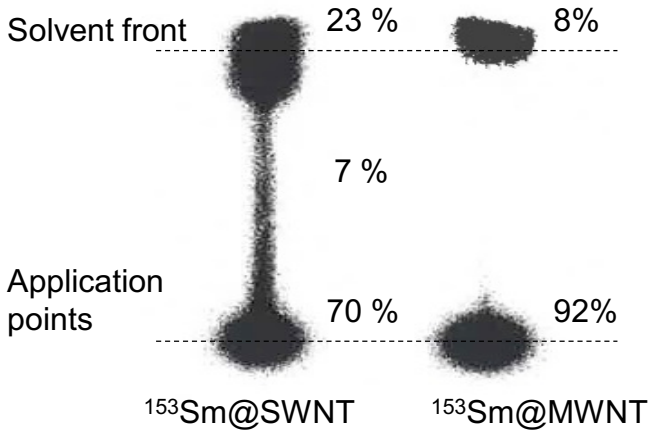

Figure S4. ITLC analysis of ^{153}Sm@SWNT and ^{153}Sm@MWNT following neutron irradiation of ^{152}Sm@SWNT and ^{152}Sm@MWNT respectively. Signals at the application point represent the stably encapsulated radionuclides.

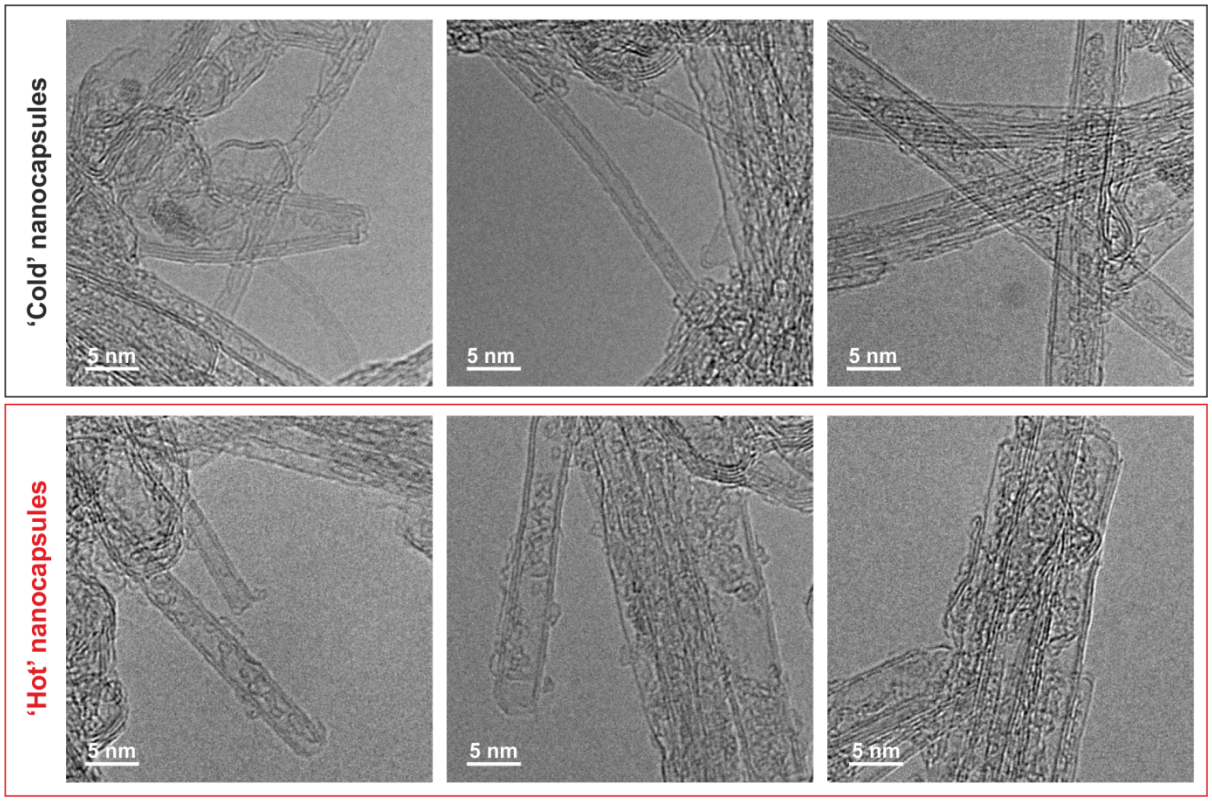

Figure S5. HRTEM images of Sm-filled SWNTs before ('Cold' nanocapsules) and after ('Hot' nanocapsules) irradiation.

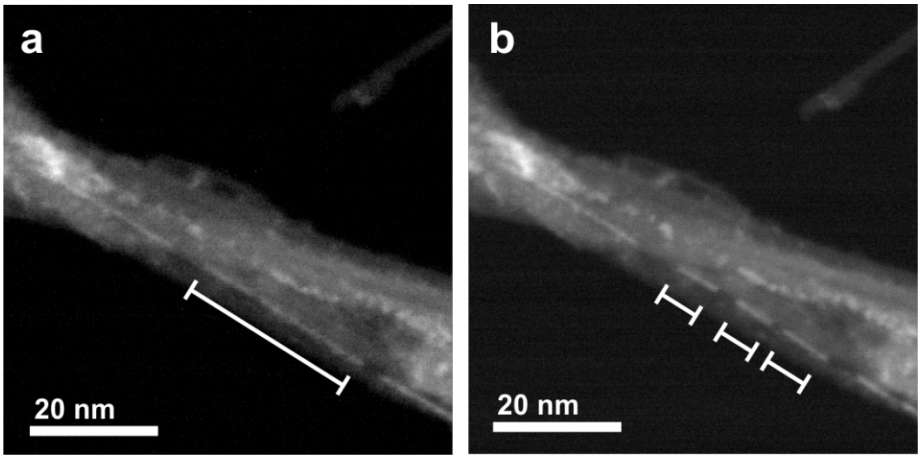

Figure S6. HAADF STEM images of a $^{152}SmCl_3$@SWNT showing that during electron microscopy observation the filling material displaces inside the SWNT. a) Initially acquired image and b) an image of the same area acquired after ca. 30 seconds. Displacement of the filling material is indicated with white bars.

Table S3. Neutron activated isotopes (of clinical interest) loaded onto nanocarriers.

Nanocarrier	Stable isotope	Neutron irradiation time	Neutron flux ($n \cdot cm^{-2} \cdot s^{-1}$)	Reported radioactivity[a]	Specific radioactivity[b] (MBq/mg)	Ref.
MWNT	^{152}Sm	96 h	$1.6x10^{14}$	11.37 GBq/mg	11370.0	This work
SWNT	^{152}Sm	96 h	$1.6x10^{14}$	6.33 GBq/mg	6330.0	This work
C_{82}	^{165}Ho	1 min	$4.3x10^{14}$	16.13 μCi/mg	0.6	3
MCN	^{165}Ho	10 h	$5.5x10^{12}$	208 μCi/100 μg	77.0	4
HoIG	^{165}Ho	0.45 h	$7.0x10^{12}$	250 μCi/mg	9.3	5
Silica NPs	^{165}Ho	1 h	$3.5x10^{12}$	213.6 μCi/mg	7.9	6
Silica NPs	^{165}Ho	2.2 h[c]	$5.5x10^{12}$	129 MBq/10.7 mg	12.1	7
Silica NPs	^{165}Ho	2 h	$5.5x10^{12}$	150 μCi/mg	5.6	8
Silica NPs	^{165}Ho	3 h	$7.7x10^{12}$	300 μCi/mg	11.1	8
AcAc	^{165}Ho	13 min	$5.5x10^{12}$	0.25 mCi/10 mg	0.9	9
AcAc	^{165}Ho	1 h	5.0×10^{12}	600 MBq/50 mg	12.0	10
PLLA	^{165}Ho	1 h	1.1×10^{13}	27.4 GBq/g	27.4	11

MWNT: Multi-walled carbon nanotubes; SWNT: Single-walled carbon nanotubes; C_{82}: Endohedral Metallofulerenes; HoIG: Holmium iron garnet; NPs: Nanoparticles; MCN: Mesoporous carbon nanoparticles; AcAc: NPs from acetylacetonate; PLLA: Poly-L-lactide

NOTES: [a]Values as reported in the reference provided

[b]Specific radioactivities calculated from "Reported activity"

[c]Irradiation up to 18h was performed but the resulting activity is not reported

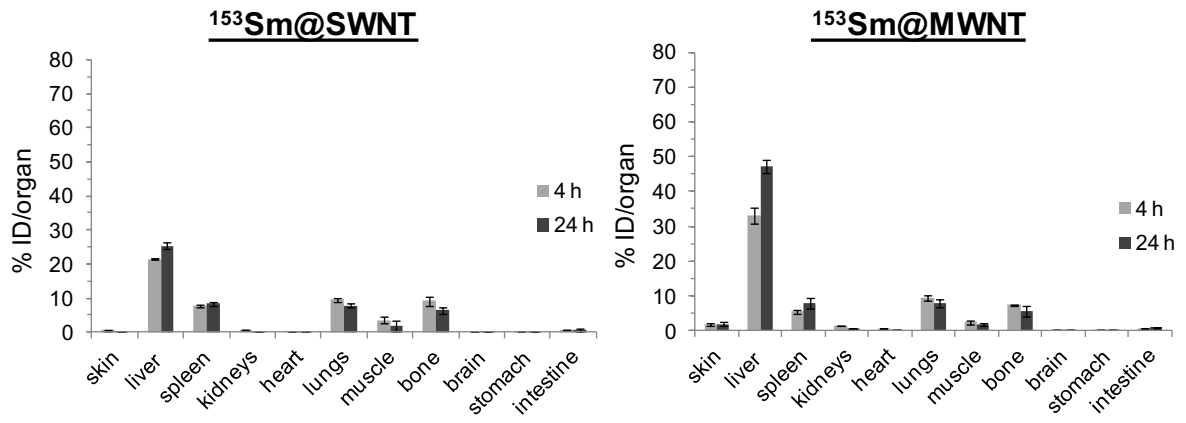

Figure S7. Tissue biodistribution of ^{153}Sm@SWNT and ^{153}Sm@MWNT (presented as %ID per organ). C57/Bl6 mice were i.v. injected with 200 μg of ^{153}Sm@SWNT or ^{153}Sm@MWNT (~1 MBq). The radioactivity of major organs sampled at specified time points were measured by γ-scintigraphy. The results are expressed as % ID/organ and presented as mean ± S.D. (n=3-4).

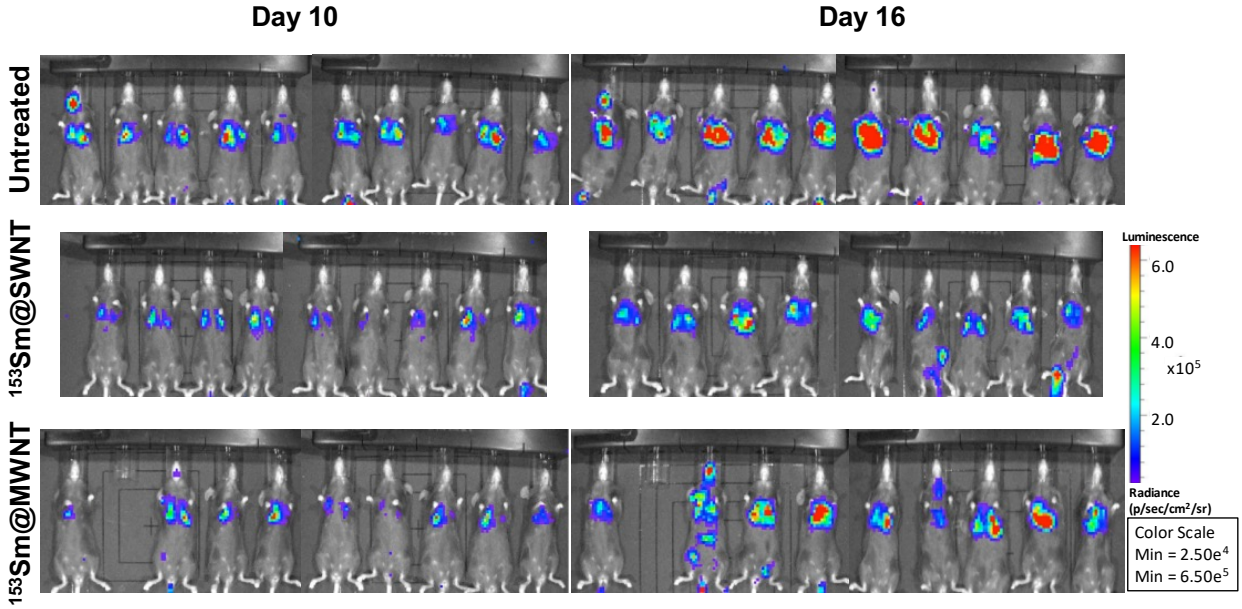

Figure S8. Live bioluminescence images of untreated mice or mice treated with ^{153}Sm@SWNT or ^{153}Sm@MWNT. B16F10-Luc tumor-bearing mice were i.v. injected with 20 MBq in 200 μg of ^{153}Sm@SWNT or ^{153}Sm@MWNT on day 8 post-tumor inoculation. Bioluminescence signals correspond to metabolic activity of luciferase-expressing B16F10 cells in the lung.

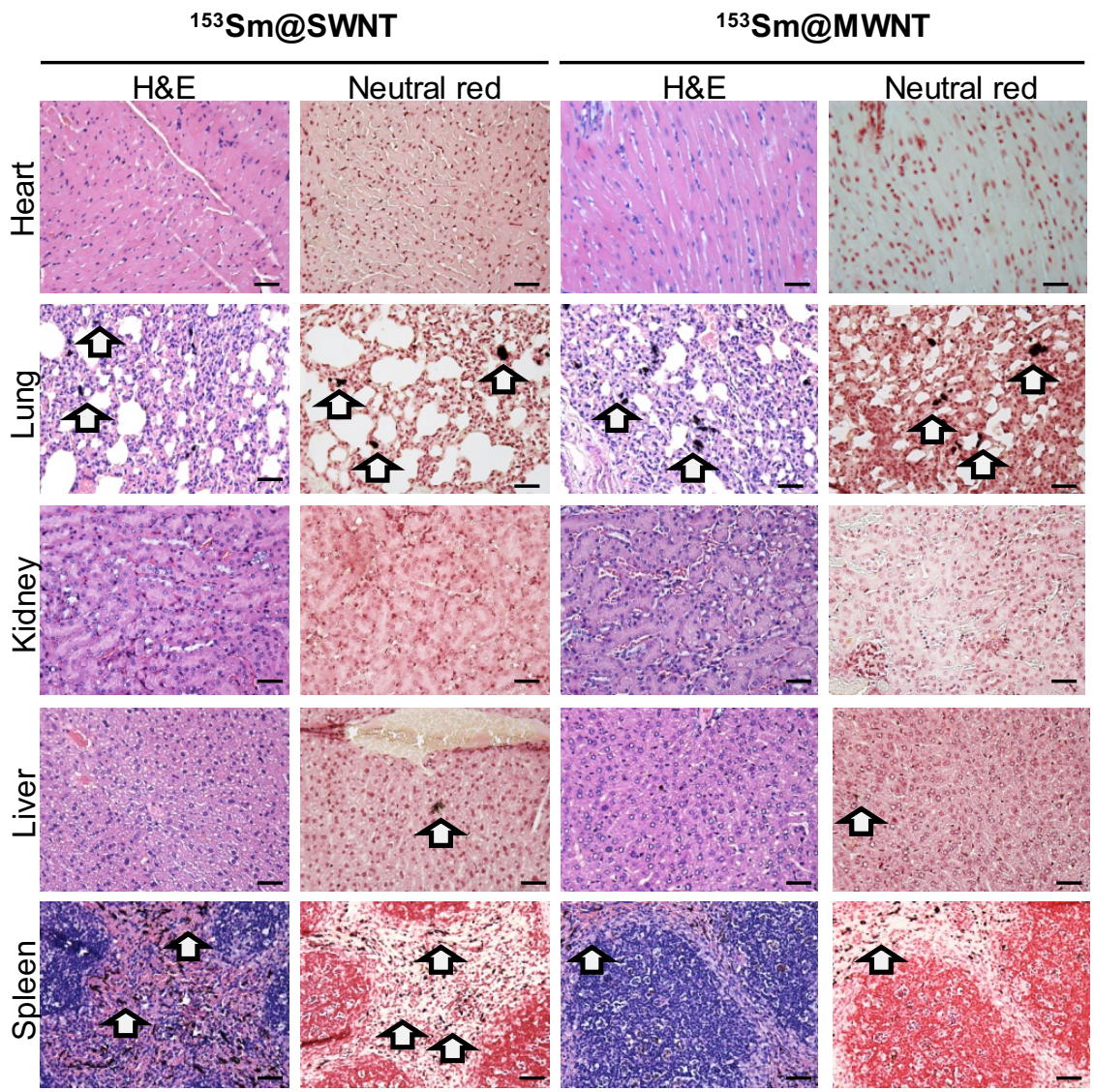

Figure S9. Histological examination of major organs from C57BL/6 mice at 24 h post injection of ^{153}Sm@SWNT and ^{153}Sm@MWNT. C57BL/6 mice were i.v. injected with 200 μg of ^{153}Sm@SWNT or ^{153}Sm@MWNT (~1 MBq). At 24 h post injection, heart, lung, kidney, liver, and spleen were excised and formalin-fixed, stained with H&E (for tissue necrosis) or Neutral Red (for CNT visualization). As a guide to the eye arrows point to some CNT aggregates. Scale bars: 50 μm.

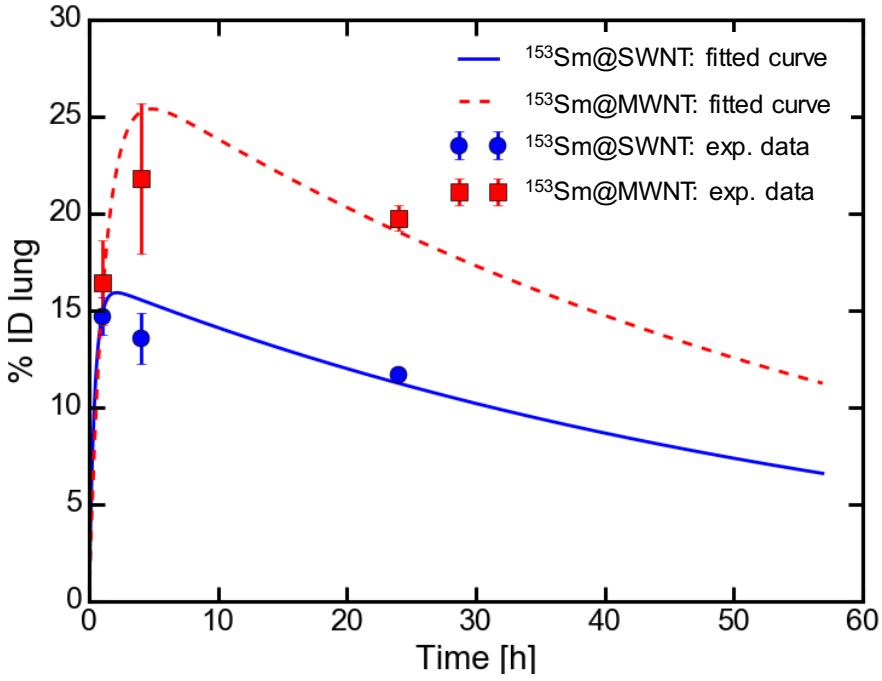

Figure S10. Fit of the experimental biodistribution data (% ID) in the lung using equation 3 described in the manuscript. Fitted parameters are $\mathrm{ID}_0 = 16.6\,\%$, $k = 0.0162\,\mathrm{h}^{-1}$ $m = 2.32\,\mathrm{h}^{-1}$ for SWNT, and $\mathrm{ID}_0 = 28.0\,\%$, $k = 0.0160\,\mathrm{h}^{-1}$ $m = 0.826\,\mathrm{h}^{-1}$ for MWNT. Experimental data are presented by circle or square dots. Lines (solid or dotted) are the fitted curve calculated using equation 3.

Experimental Details

Materials and Reagents: Chemical vapor deposition (CVD) Elicarb® SWNTs and MWNTs were supplied by Thomas Swan & Co. Ltd (UK) as a solid powder. The SWNT material also contains a fraction of few-walled carbon nanotubes, mainly double-walled. Enriched $^{152}Sm_2O_3$ were provided by CIS-Bio International-Ion Beam Applications (France). Hydrogen peroxide, sulphuric acid and nitric acids were purchased from Panreac AppliChem (Spain) for CNT pre-treatment. Instant thin layer chromatography paper impregnated with silica gel (ITLC-SG) was obtained from Agilent Technologies (UK). Isoflurane for anesthesia was purchased from Abbott (IsoFlo®, Abbott Laboratorie Ltd, UK).

Purification and Shortening of CNTs: Both SWNTs and MWNTs were initially treated to shorten the tubes, open their ends and remove carbonaceous and metallic (catalyst) impurities. SWNTs were exposed to a combined piranha-steam treatment, whereas MWNTs underwent a combined H_2SO_4:HNO_3-steam treatment following previously reported protocols.[12]

Synthesis of $^{152}SmCl_3$ from $^{152}Sm_2O_3$: Enriched $^{152}Sm_2O_3$ was transformed to anhydrous $^{152}SmCl_3$ following the protocol reported for the synthesis of anhydrous $SmCl_3$ with natural isotopic distribution (non-enriched).[13] The synthesis of the anhydrous metal halide was performed by dissolution of the enriched metal oxide in HCl, followed by dehydration of the collected solid at 240 °C under dynamic vacuum. The synthesized anhydrous $^{152}SmCl_3$ is highly hygroscopic and was handled under an inert atmosphere.

Filling of CNTs with $^{152}SmCl_3$: Cut and purified SWNT (100 mg) or MWNT (200 mg) and $^{152}SmCl_3$ were ground together in a weight ratio 1:10 (CNTs:$^{152}SmCl_3$). The materials were ground using an agate mortar and pestle inside an argon filled glove box until the mixture presented a uniform color. The samples were split in smaller fractions, placed inside silica tubes and sealed under vacuum. The resulting silica ampoules were placed inside a horizontal tubular furnace and annealed for 12 h at 900 °C (SWNT) or 1200 °C (MWNT) thus leading to the formation of carbon nanocapsules (closed-ended filled CNTs). The samples were recovered from the ampoules and the non-encapsulated material, external to the CNTs was dissolved and washed away. The removal of the external material was followed by UV-Vis spectroscopy of the

collected filtrates, until no more $^{152}SmCl_3$ was detected in the washings.[14] Initially the filled nanotubes were soaked in 200 mL of water containing 0.6 M HCl. The sample was then collected by filtration over a 0.2 μm polycarbonate membrane. This "pre-washing" step was followed by washing the sample three times in 200 mL acidic water at 80 °C for 24 h under constant stirring each time. The sample was collected by filtration between washings. A final washing step was performed using 200 mL of pure water, without the addition of HCl, whilst keeping the rest parameters constant. The collected solid powder was dried at 80 °C overnight.

Neutron activation of ^{152}Sm-filled CNTs: Vacuum sealed silica ampoules containing 30 mg of either ^{152}Sm@SWNT or ^{152}Sm@MWNT were placed in an aluminum capsule, weighed down with a lead-weight in a pool-type reactor (OSIRIS, CEA Saclay, France) and irradiated at a neutron flux of $1.6x10^{14}$ n·cm^{-2}·s^{-1} for 96 h. The irradiation protocol was established according to equation (1):[15]

$$A = \frac{0.6\sigma\Phi}{M}\left(1 - e^{-\lambda t}\right) \qquad (1)$$

where A is the predicted activity of the radioisotope produced (Bq g^{-1}), M is the atomic mass of the target element (152 g mol^{-1} for ^{152}Sm), Φ is the neutron flux of the reactor ($1.6x10^{14}$ n cm^{-2}s^{-1}), σ is the thermal neutron activation cross-section of the target isotope (206 barns for ^{153}Sm), λ is the decay constant ($0.693/T_{1/2}$), ($T_{1/2}$ is the half life of the target isotope, which is 46.27 h for ^{153}Sm) and *t* is the irradiation time (96 h). The value of A for the given conditions can then be used to make a prediction of the nanotubes, by factoring in the mass of nanotubes and the corresponding percentage content of ^{152}Sm that was measured before the irradiation.

After removing the ampoules from the pool, they were allowed to cool down, removed from the aluminum casing, and then transferred to CIS bio International, Saclay (France) where they were processed in a fully sealed radioprotection hot cell. Radioactivity was measured using a dose calibrator (VDC 404, Veenstra Instruments, The Netherlands). The ampoules were then shattered and the contents (^{153}Sm@SWNT and ^{153}Sm@MWNT powders) were separately suspended in a volume of 1% Pluronic® F-127 saline (0.9 % NaCl) solution, using sonication such to produce a suspension with a loading of 0.5 mg/mL. The glass fragments from the broken silica ampoule were separated from the bulk of the suspension by sedimentation. Large aggregates of ^{153}Sm@CNTs were also precluded in this way. In order to transfer this product to the *in vivo*

facilities in vials, keeping within their local limits of activity handling, only a fraction of this suspension was then separated into a final vial, which was then shipped and arrived in a few days. On arrival, a sonication and a series of dilution steps were performed to ensure that the final dispersion injected in mice was physically stable and free of aggregates, as detailed in the *in vivo* section.

Quantification of $^{152}SmCl_3$ filling yields by ICP-MS: As a analytical validation measure, each carbon nanotube sample was subdivided into fractions of different sizes in the range of 1-15 mg, and was weighed three times on a pre-calibrated analytical balance. The samples were then added to a PTFE-TFM reactor in an Anton Paar Multiwave 3000, fitted with an 8SXF100 rotor. 6 mL 65% Suprapur® nitric acid (Merck KGaA, Germany), and then 2 mL of 30% Suprapur® hydrogen peroxide (Merck KGaA, Germany) were dispensed from calibrated micropipettes and the microwave digestion was completed by applying 800 W for 40 minutes, with an initial ramp of 5 min. The contents of each reactor were then transferred to a polyproylene flask, followed by a series of washings with de-ionised water (ELGA Labwater PURELAB® Classic water purifying system; resistivity 18.2 MΩ/cm), and the volume was then made up to 25 mL. Two additional control solutions were prepared and analyzed. It was demonstrated that no impurities were introduced during this process using a "preparation blank," consisting of all of the reagents except the nanotubes, that was passed through the microwave at the same time as the actual samples. It was also confirmed that all of the material that was added to the reactors was recovered by preparing a solution from the final washing. Prior to analysis by ICP-MS, all of the samples were filtered with a 33 mm 0.22 μm MILLEX ® GV PVDT filter.

ICP-MS analysis was carried out at Cis Bio International using an ICP-MS with a quadrupole collision cell (PerkinElmer Sci EX ELAN® DRC II). The system check consisted of: a daily performance report using a standard reference solution of magnesium, indium, uranium, cerium and barium, with relative standard deviations (RSD) within 0.4 to 1.1% of the anticipated value. The sample sequence then consisted of triplicate injections of: a blank containing de-ionized water, the "preparation blank" and then the actual samples, separated by injections of de-ionized water. The quantification was performed using an external ^{152}Sm calibration standard. The stability of the measurements was monitored by spiking each sample with an identical level of a rhodium standard of 5 ppb and this gave RSDs of less than 1%. The range of concentrations

chosen for the ^{152}Sm calibration depended on the particular sample and covered the ranges of either 1 to 5 ppb or 1 to 30 ppb, and all of Pearson correlation coefficients R^2 coefficients were greater than 0.9999. The results corresponding to the overall % ^{152}Sm were then reported to one decimal place.

Electron microscopy: HAADF-STEM images were acquired at 20 kV on an FEI Magellan XHR Scanning Electron Microscope (SEM) with the use of a specially adapted detector. HRTEM images were acquired on a FEI Tecnai G2 F20 microscope at 200 kV. Samples were dispersed in ethanol and deposited onto lacey carbon Cu grids. ^{153}Sm@CNT were imaged after the complete decay of radioactivity. EDX was carried out on a FEI Quanta SEM microscope equipped with an EDAX detector at 20 kV.

Animals: All *in vivo* experiments were conducted under the authority of project and personal licenses granted by the UK Home Office and the UKCCCR Guidelines (1998). Female C57BL/6 mice aged 6-8 weeks were purchased from Harlan (UK) and used for all *in vivo* studies.

ITLC examination of ^{153}Sm@CNTs: ITLC was performed to examine whether there was free ^{153}Sm present in the ^{153}Sm@CNT suspensions (neutron irradiated ^{152}Sm@CNT) prior to injection. Aliquots of ^{153}Sm@SWNT and ^{153}Sm@MWNT were spotted on TLC strips and then developed in 0.1 M ammonium acetate containing 50 mM EDTA as a mobile phase. Strips were allowed to dry and counted quantitatively using a cyclone phosphor detector (Packard Biosciences, UK).

Preparation of ^{153}Sm-CNTs for in vivo studies: The ^{153}Sm@CNT suspensions underwent different dilutions to contain the appropriate radioactivity for different *in vivo* studies. The dilution was carried out by mixing the ^{153}Sm@CNT dispersions with different amounts of non-irradiated ^{152}Sm@CNT suspensions (2 mg/mL in 1% Pluronic® F-127 saline). The resulting mixture was then sonicated for 10-15 min. Each injection dose, either for imaging, biodistribution or therapy studies, contained the same amount of CNT (200 μg), but possessed different radioactivity which are specified in their experimental sections accordingly. Injection suspensions were added with 0.1 M EDTA (one twentieth of the injection volume) to chelate any free ^{153}Sm.

In vivo SPECT/CT imaging of ^{153}Sm@CNT following i.v. injection: The biodistribution of ^{153}Sm@CNTs was firstly assessed by 3D whole body SPECT/CT imaging. Mice were anaesthetized by isoflurane inhalation during imaging. Each injection dose for ^{153}Sm@SWNT or

^{153}Sm@MWNT suspensions contained approximately 10 MBq. Injection suspensions were added with 0.1 M EDTA (one twentieth of the injection volume) to chelate free ^{153}Sm. Immediately after injection, and at 4 h and 24 h, mice were imaged using the Nano-SPECT/CT scanner (Bioscan, USA). SPECT images of each mouse were taken in 24 projections over 30-40 min using a four-head scanner with 1.4 mm pinhole collimators. CT scans were performed at the end of each SPECT acquisition. All images were reconstructed by MEDISO software (Medical Imaging Systems), and SPECT and CT images were merged using the InVivoScope™ software (Bioscan, USA).

Pharmacokinetics and organ biodistribution of ^{153}Sm@CNTs by γ-scintigraphy: Mice anaesthetized by isoflurane inhalation were injected with ^{153}Sm@SWNT or ^{153}Sm@MWNT suspensions *via* a tail vein. Each injection dose of ^{153}Sm@SWNT or ^{153}Sm@MWNT suspensions contained approximately 0.8 MBq. Blood was sampled from a tail vein at 5 min, 30 min, 4 h or 24 h after injection. At 4 h and 24 h, mice were sacrificed and major organs were excised and weighed. To assess the excretion profiles, animals were housed individually in metabolic cages where the mice have free access to water but not food. Urine and feces were collected over 24 h after injection. The radioactivity of each sample (*i.e.* tissues, blood, urine or feces) was measured by γ-scintigraphy (LKB Wallac 1282 Compugamma, PerkinElmer) and the results were expressed as percentage injection dose per sample (% ID) or per g of sample (% ID/g). Collected organs were fixed in 10% neutral buffered formalin for histological examination.

B16F10-Luc lung metastasis tumor model: Mice anaesthetized by isoflurane inhalation were injected with 5 x 10^5 B16F10-Luc cells in 0.2 mL of PBS *via* a tail vein to establish pulmonary melanoma metastases. Following tumor inoculation, *in vivo* quantitative bioluminescence imaging was performed on day 7, 10, 13 and 16 to monitor the tumor growth (IVIS Lumina III, Perkin-Elmer, UK). Mice under anesthesia were subcutaneously injected with luciferin (D-luciferin potassium salt, Perkin-Elmer, UK) at 150 mg/kg and imaged 10 min after injection. Bioluminescence signals from regions of interests were measured using Living Image software (Perkin-Elmer, UK) and recorded as total flux (photons/sec).

In vivo ^{153}Sm@CNT radiotherapy studies: To determine the radiotherapeutic action of ^{153}Sm@SWNT and ^{153}Sm@MWNT, B16F10-Luc tumor bearing C57BL/6 mice were randomly divided into three groups (n = 10): untreated, ^{153}Sm@SWNT and ^{153}Sm@MWNT. On day 8 post

tumor inoculation, mice were intravenously injected with 200 μg of ^{153}Sm@SWNT or ^{153}Sm@MWNT suspensions containing approximately 20 MBq. Mice were sacrificed on day 16 post tumor inoculation, and major organs including lung, liver, spleen, heart, and kidney were weighed and fixed in 10% neutral buffered formalin for histological examination. Tumor growth was monitored by bioluminescence imaging as described previously. The tumor growth data was expressed as mean ± SEM (standard error of the mean), with *n* denoting the number of animals. Significant differences were examined using one-way ANOVA followed by Tukey's multiple comparison test. *: $p < 0.05$; ***: $p < 0.001$

Histological examination: Major organs excised from the mice in the biodistribution study (*i.e.* 24 h post injection) and from the mice after ^{153}Sm@CNT radiotherapy were subjected to histological examination. Harvested fixed organs were paraffin-embedded and sectioned for haematoxylin and eosin (H&E) or Neutral Red staining according to standard histological protocols at the Royal Veterinary College (UK). All stained sections were analysed using a Leica DM 1000 LED Microscope (Leica Microsystems, UK) coupled with a CCD digital camera (Qimaging, UK).

References

1. Hong, S. Y.; Tobias, G.; Al-Jamal, K. T.; Ballesteros, B.; Ali-Boucetta, H.; Lozano-Perez, S.; Nellist, P. D.; Sim, R. B.; Finucane, C.; Mather, S. J.; Green, M. L. H.; Kostarelos, K.; Davis, B. G. Filled and Glycosylated Carbon Nanotubes for *In Vivo* Radioemitter Localization and Imaging. *Nat. Mater.* **2010**, *9*, 485-490.
2. Ge, H.; Riss, P. J.; Mirabello, V.; Calatayud, D. G.; Flower, S. E.; Arrowsmith, R. L.; Fryer, T. D.; Hong, Y.; Sawiak, S.; Jacobs, R. M. J.; Botchway, S. W.; Tyrrell, R. M.; James, T. D.; Fossey, J. S.; Dilworth, J. R.; Aigbirhio, F. I.; Pascu, S. I. Behavior of Supramolecular Assemblies of Radiometal-Filled and Fluorescent Carbon Nanocapsules *In Vitro* and *In Vivo*. *Chem* **2017**, *3*, 437-460.
3. Cagle, D. W.; Kennel, S. J.; Mirzadeh, S.; Alford, J. M.; Wilson, L. J. *In Vivo* Studies of Fullerene-Based Materials Using Endohedral Metallofullerene Radiotracers. *Proc. Natl. Acad. Sci. U. S. A.* **1999**, *96*, 5182-5187.
4. Kim, J.; Luo, Z.-X.; Wu, Y.; Lu, X.; Jay, M. *In-Situ* Formation of Holmium Oxide in Pores of Mesoporous Carbon Nanoparticles as Substrates for Neutron-Activatable Radiotherapeutics. *Carbon* **2017**, *117*, 92-99.
5. Munaweera, I.; Shi, Y.; Koneru, B.; Saez, R.; Aliev, A.; Di Pasqua, A. J.; Balkus, K. J. Chemoradiotherapeutic Magnetic Nanoparticles for Targeted Treatment of Nonsmall Cell Lung Cancer. *Mol. Pharm.* **2015**, *12*, 3588-3596.

6. Munaweera, I.; Koneru, B.; Shi, Y.; Pasqua, A. J. D.; Kenneth J. Balkus, J. Chemoradiotherapeutic Wrinkled Mesoporous Silica Nanoparticles for Use in Cancer Therapy. *APL Mater*. **2014**, *2*, 113315.
7. Di Pasqua, A. J.; Yuan, H.; Chung, Y.; Kim, J. K.; Huckle, J. E.; Li, C.; Sadgrove, M.; Tran, T. H.; Jay, M.; Lu, X. Neutron-Activatable Holmium-Containing Mesoporous Silica Nanoparticles as a Potential Radionuclide Therapeutic Agent for Ovarian Cancer. *J. Nucl. Med*. **2013**, *54*, 111-116.
8. Di Pasqua, A. J.; Miller, M. L.; Lu, X.; Peng, L.; Jay, M. Tumor Accumulation of Neutron-Activatable Holmium-Containing Mesoporous Silica Nanoparticles in an Orthotopic Non-Small Cell Lung Cancer Mouse Model. *Inorg. Chim. Acta* **2012**, *393*, 334-336.
9. Di Pasqua, A. J.; Huckle, J. E.; Kim, J.-K.; Chung, Y.; Wang, A. Z.; Jay, M.; Lu, X. Preparation of Neutron-Activatable Holmium Nanoparticles for the Treatment of Ovarian Cancer Metastases. *Small* **2012**, *8*, 997-1000.
10. Bult, W.; Varkevisser, R.; Soulimani, F.; Seevinck, P. R.; de Leeuw, H.; Bakker, C. J. G.; Luijten, P. R.; van het Schip, A. D.; Hennink, W. E.; Nijsen, J. F. W. Holmium Nanoparticles: Preparation and *In Vitro* Characterization of a New Device for Radioablation of Solid Malignancies. *Pharm. Res*. **2010**, *27*, 2205-2212.
11. Hamoudeh, M.; Fessi, H.; Salim, H.; Barbos, D. Holmium-Loaded PLLA Nanoparticles for Intratumoral Radiotherapy *via* the TMT Technique: Preparation, Characterization, and Stability Evaluation after Neutron Irradiation. *Drug Dev. Ind. Pharm*. **2008**, *34*, 796-806.
12. Kierkowicz, M.; Pach, E.; Santidrián, A.; Sandoval, S.; Gonçalves, G.; Tobías-Rossell, E.; Kalbáč, M.; Ballesteros, B.; Tobias, G. Comparative Study of Shortening and Cutting Strategies of Single-Walled and Multi-Walled Carbon Nanotubes Assessed by Scanning Electron Microscopy. *Carbon* **2018**, *139*, 922-932.
13. Martincic, M.; Frontera, C.; Pach, E.; Ballesteros, B.; Tobias, G. Synthesis of Dry $SmCl_3$ from Sm_2O_3 Revisited. Implications for the Encapsulation of Samarium Compounds into Carbon Nanotubes. *Polyhedron* **2016**, *116*, 116-121.
14. Martincic, M.; Pach, E.; Ballesteros, B.; Tobias, G. Quantitative Monitoring of the Removal of Non-Encapsulated Material External to Filled Carbon Nanotube Samples. *Phys. Chem. Chem. Phys*. **2015**, *17*, 31662-31669.
15. *Manual for Reactor Produced Radioisotopes, Iaea-Tecdoc-1340*. Vienna, Austria, **2003**, 189-192.